

Contents lists available at ScienceDirect

Journal of Energy Chemistry

journal homepage: www.elsevier.com/locate/jechem



http://www.journals.elsevier.com/ iournal-of-energy-chemistry

Atomically dispersed catalysts for small molecule electrooxidation in direct liquid fuel cells

Jinfa Chang^a, Guanzhi Wang^{a,b}, Wei Zhang^{a,b}, Yang Yang^{a,b,c,*}

- ^a NanoScience Technology Center, University of Central Florida, Orlando, FL 32826, USA
- ^b Department of Materials Science and Engineering, University of Central Florida, Orlando, FL 32826, USA
- ^cDepartment of Chemistry, Renewable Energy and Chemical Transformation Cluster, University of Central Florida, Orlando, FL 32826, USA

ARTICLE INFO

Article history: Received 30 July 2021 Revised 7 December 2021 Accepted 8 December 2021 Available online 16 December 2021

Keywords: Atomic dispersion Electrocatalyst Small molecule electrooxidation Direct liquid fuel cells

ABSTRACT

Direct liquid fuel cells (DLFCs) have received increasing attention because of their high energy densities, instant recharging abilities, simple cell structure, and facile storage and transport. The main challenge for the commercialization of DLFCs is the high loading requirement of platinum group metals (PGMs) as catalysts. Atomically dispersed catalysts (ADCs) have been brought into recent focus for DLFCs due to their well-defined active sites, high selectivity, maximal atom-utilization, and anti-poisoning property. In this review, we summarized the structure–property relationship for unveiling the underlying mechanisms of ADCs for DLFCs. More specifically, different types of fuels used in DLFCs such as methanol, formic acid, and ethanol were discussed. At last, we highlighted current challenges, research directions, and future outlooks towards the practical application of DLFCs.

© 2021 Science Press and Dalian Institute of Chemical Physics, Chinese Academy of Sciences. Published by ELSEVIER B.V. and Science Press. All rights reserved.

1. Introduction

Energy dilemma is believed to be one of the biggest challenges/ needs to be resolved in the following decades or longer [1]. Most of the world's energy need has largely relied on unsustainable fossil fuels, which provide great convenience to our life. On the other hand, we are facing big challenges due to environmental concerns related to the emission of hazardous chemicals. It is urgent to discover and develop new, accessible, and reproducible energy storage and conversion technologies for the replacement of conventional sources with clean, highly efficient, easily operational, and environmentally friendly energy systems. Hydrogen (H₂)-fed polymer electrolyte membrane fuel cells (H₂-PEMFCs) have shown enormous promise in the automobile industry [2]. However, the high pressure needed during operation may result in explosion accident if the H₂ is not handled properly. Besides, the transport and storage of H₂ are still big challenges due to the highly flammable nature of H₂. On the contrary, compared with H₂-PEMFCs, direct liquid fuel cells (DLFCs) using small organic molecules (e.g., methanol, ethanol, formic acid, etc.) as alternative fuels at the anode, can effectively resolve the storage and transportation problems [3,4].

There are quite many types of small liquid molecules that can be used as anode fuels in DLFCs (Table S1). However, the strong chemical bonds in these small molecules, especially the C–C bond, are difficult to be cleaved. Hence, attention is mainly focused on small molecular fuels containing C_1 and C_2 such as methanol, formic acid, and ethanol as the most representative ones. Liquid fuels, such as ethanol, are renewable and can be easily acquired in large quantities from biomass [5]. In contrast, more than 95% of industrial hydrogen is obtained from coal gasification and steam methane reforming [6]. Moreover, liquid fuels possess severalfold higher volumetric energy density than hydrogen (Fig. 1a). Thus, the DLFCs show promising applications in portable power when considering the much more economic benefit and higher safety than H_2 -PEMFCs [7,8].

Despite the DLFCs showing comparable theoretical voltage (Fig. 1b) with H_2 -PEMFCs, the complete oxidation of liquid small molecules requires much more electrons (Fig. 1c) to facilitate the cleavage of the C–H bond and/or C–C bond, leading to slower anode reaction kinetics in the DLFCs than H_2 -PEMFCs. On the other hand, the loss of overpotential for H_2 -PEMFCs and DLFCs is mainly from the sluggish oxygen reduction reaction (ORR) at the cathode and slow reaction kinetics for small molecule oxidation at the anode, respectively. Therefore, most research attention has been focused on developing efficient ORR catalysts for H_2 -PEMFCs, while the research for DLFCs was mainly to accelerate the reaction kinetics, restrain the catalyst poisoning, and realize the complete fuel

^{*} Corresponding author.

E-mail address: Yang.Yang@ucf.edu (Y. Yang).

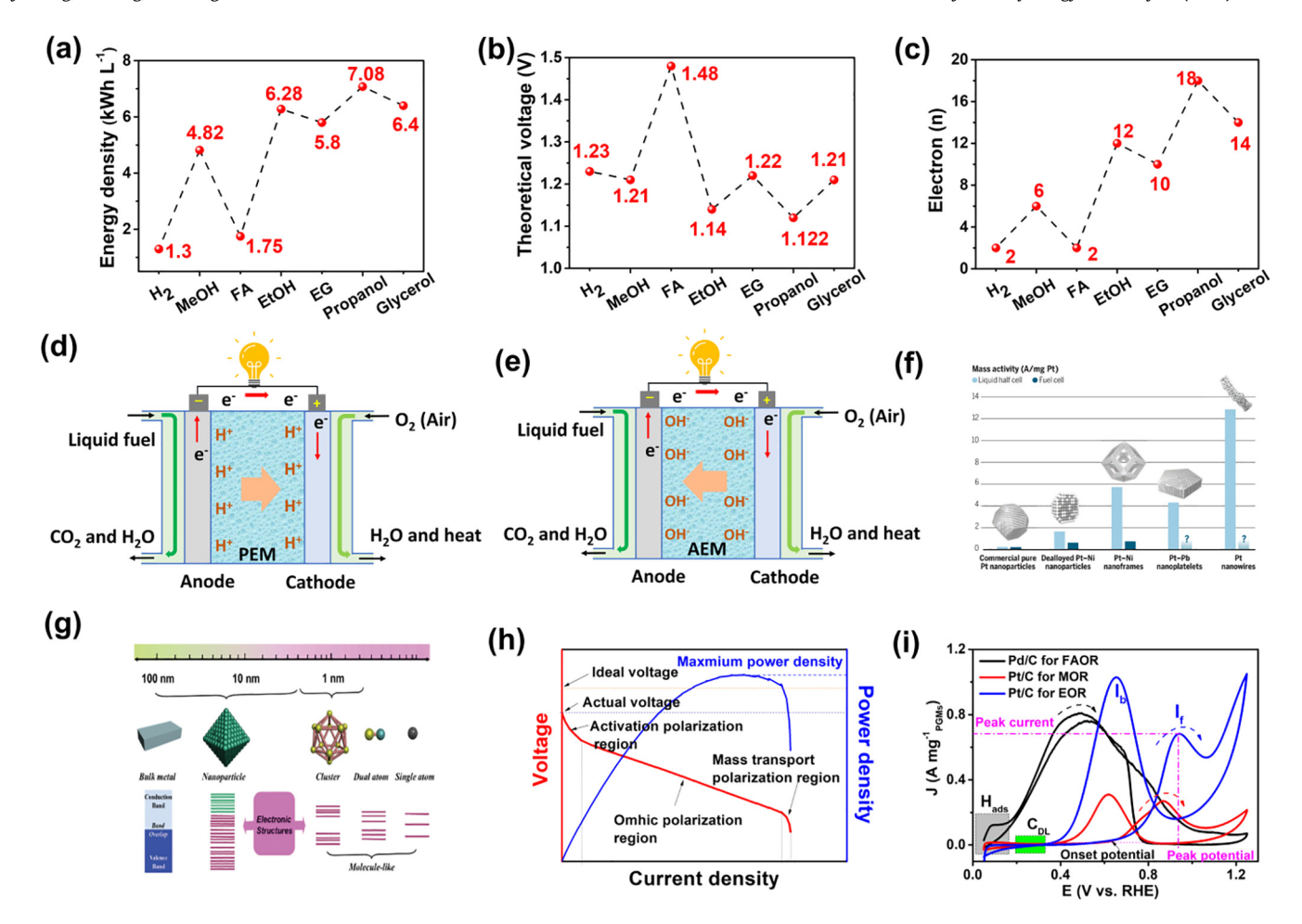


Fig. 1. The fundamentals, configurations, and structure-performance relationship of DLFCs. (a) The energy density of H₂ and typical liquid fuels. (b) The ideal voltage (c) and the number of electron transfers need for complete oxidation of H₂ and typical liquid fuels. MeOH, methanol; FA, formic acid; EtOH, ethanol; EG, ethylene glycol. Schematic of (d) PEM and (e) AEM-based DLFCs. (f) The cathode ORR catalytic activity of the representative catalyst from liquid three-electrode half-cell to the real H₂-O₂ fuel cell. Adapted with permission from Ref. [37]. Copyright 2016 AAAS. (g) The geometric and electronic structures of materials from bulk, NPs, to single atoms. Adapted with permission from Ref. [44]. Copyright 2020, RSC. (h) Typical polarization and power density curves for DLFCs. (i) Typical anode cyclic voltammetry (CV) of Pd/C and Pt/C for formic acid, methanol, and ethanol oxidation, the figure was redrawn from Refs. [15,16,76].

oxidation at the anode side. Since extensive reviews have reported the issues on ORR for H_2 -PEMFCs [7–13], which are also applied to the cathode reactions in DLFCs, we will primarily stress the anode reactions for the DLFCs in this review.

The DLFCs show apparent advantages in micro/middle-size powers from hundred watts to kilowatts [14], which can be used for portable power and military purposes. The DLFCs can be directly operated without an outward electrical power supply and provide a much longer conversation time than lithium-ion batteries. In DLFCs (Fig. 1d and e), the liquid fuel is fed into the anode for the oxidation reactions, and oxygen/air is injected into the cathode for the ORR. To make the reactions go without a hitch, efficient catalysts are needed to lower the activation energy for both anode and cathode reactions. Till now, the most efficient catalysts are platinum group metals (PGMs)-based materials, such as Pt, Pd, Au, Ru, Ir, and their alloys [15-21]. And high PGMs loading is required to ensure sufficient power density and stability [22]. For example, for the direct methanol fuel cell (DMFC), PtRu alloy was recognized as the best catalyst for the methanol electrooxidation reaction at the anode [23,24], and Pt was the best choice for the ORR at the cathode [25-27]. The maximum peak power density of 50 mW cm⁻² was obtained by using 2 mg_{PtRu} cm⁻² at the anode and 4 mg_{Pt} cm⁻² at the cathode for single DMFCs [24,25], which is higher than other types of catalysts [15,23]. While for direct formic

acid fuel cell (DFAFC), the single-cell power density of $550~\text{mW}~\text{cm}^{-2}$ was obtained with a high loading of $1.2~\text{mg}_{\text{Pd}}~\text{cm}^{-2}$ at the anode and $4~\text{mg}_{\text{Pt}}~\text{cm}^{-2}$ at the cathode [16]. However, the price of present DLFCs technology is still incapable of matching the DOE's recent target and ultimate goal [28]. Thus, it is critical to reducing the catalysts loading and maximizing the atomutilization of PGMs to push the DLFCs commercialization.

Most advanced energy storage/conversion technologies largely rely on efficient catalysis, which is the most cost-effective, energy-saving, and environmentally friendly approach to largescale utilization of sustainable energy [29,30]. Because of the dominant role of catalysis in fuel cells, the rational design and highthroughput synthesis of highly stable and efficient catalysts are enormously important. Moreover, the price of the catalyst layer accounts for the major fuel cells cost [31,32], which is considerably more expensive than other parts such as bipolar plates, membrane frame/gaskets, gas diffusion layer, polymer electrolyte membrane, and so on. Thus, the core task of fuel cells development is to reduce the amount of PGMs usage or switch to non-PGMs alternatives [11,33]. Unfortunately, the state-of-the-art catalysts are still PGMs-based materials [4], especially for the anode oxidation reactions in DLFCs (Tables S2 and S3). When operating the fuel cells, the high-efficiency catalysts with low loading can accelerate surface reactions by lowering the activation energy and increasing

the reaction kinetics [34]. Nowadays, heterogeneous catalysts are widely used in DLFCs, in which the metals act as catalytic active phase and are loaded on the carbon materials to ensure the relatively high specific surface area for active site exposure. Besides, nanoparticles (NPs) have much larger surface areas than their bulk counterparts, and more specifically, decreasing the particle size can greatly increase the catalytic activity due to the modified atomic and electronic structures, as well as exposing more active sites [35,36]. Up to date, nanoscale PGMs catalysts with different geometric structures and abundant active sites have shown a promising future in electrochemical energy fields. However, even with the best nano-catalysts, the performance of fuel cells achieved from laboratory-scale studies cannot be fully transferred to industrial applications (Fig. 1f) [37]. Furthermore, the small molecule electrooxidation reactions only occur on the metal catalysts' surfaces, meaning that the non-accessible metal atoms inside the catalvsts are inactive and thus wasted. Hence, the non-reaction usage of metals, including PGMs and non-PGMs, needs to be minimized as much as possible to reduce the cost of DLFCs while remaining the high catalytic performance [38].

When decreasing the size of NPs, the discrete sub-nano clusters catalysts (CCs) will be obtained [39-41]. And further decreasing the size of discrete sub-nano CCs will result in the so-called single-atom catalysts (SACs) [42,43]. As shown in Fig. 1(g) [44], both NPs and discrete sub-nano CCs have metal-metal bonds, which is absent in SACs. Conversely, the SACs are isolated on the support, which maximizes the utilization of active metals. The atomically dispersed catalysts (ADCs), including SACs and singleatom-alloy catalysts (SAACs) [45], have been brought into large exploration for small organic molecule electrooxidation reactions. Compared with the nanoscale catalysts, the ADCs separate their active sites in the form of single atoms without forming NPs or CCs [46,47]. The unique nature of ADCs can save metal resources, especially for PGMs-based metals [48-50]. Besides, compared with the nanoscale catalysts, the ADCs show extremely enhanced catalytic activity and selectivity due to the increased exposed active sites and altered electronic structure [29,42,51,52]. However, the ADCs tend to aggregate into CCs and NPs due to the increased surface energy with the decrease of particle size. To keep the atomic dispersion of ADCs adhered tightly to the supports without being agglomerated into bigger CCs or NPs, the strong metal-support interaction and the charge transfer across the interfaces should be considered. This interaction between metals and supports (or other heteroatoms) via chemical coordination enables ADCs with modified electronic structures, which are significantly different from the metal NPs [53]. The appropriate supports with good conductivity, large surface area, and plentiful defects or heteroatoms, should be used for ADCs to construct the stable configuration with atomic distribution and ensure fast electron transport during the catalytic process [49]. Till now, the carbon-based materials have been widely used as supporting matrixes in electrocatalytic reactions due to the low price, light weight, good conductivity, large surface area and easily doped by heteroatoms and anchored ADCs on the carbon surface [54-57]. Thanks to the maximized metal dispersion and almost 100% atomic utilization efficiency on the supporting matrixes, the ADCs are the most promising materials to realize the high utilization efficiency of PGM in large-scale applications. Moreover, ADCs have exhibited extraordinary electrocatalytic activities in many electrochemical reactions compared with the nano-catalysts because of their sufficiently exposed active sites and unique structural properties (Table S4).

Even though the ADCs have been widely studied and shown promising future in many electrocatalytic reactions [47,51,52,58–66] and batteries [67–70], such as ORR, oxygen evolution reaction (OER), hydrogen oxidation reaction (HOR), hydrogen evolution reaction (HER), carbon dioxide reduction reaction (CO₂RR), and

nitrogen reduction reaction (NRR), the studies on ADCs for small molecule electrooxidation reactions at the anode of DLFCs are inadequately reviewed. The underlying mechanism of ADCs in small molecule electrooxidation reactions is still not thoroughly understood. In this review, we will not focus on the synthesis methods and characterization techniques of ADCs that have been well summarized by other researchers [38,47,51,52,58–60,71]. Instead, our attention will first focus on revealing the structure-performance relation and the underlying mechanism of ADCs for small molecule electrooxidation reactions. Then we will briefly summarize and discuss the applications of ADCs on small molecule electrooxidation reactions for DLFCs. This comprehensive review will shine a light on future rational design and application of ADCs for DLFCs.

2. Fundamental, configuration, operation principle, and activity descriptors of DLFCs

The DLFCs can be classified into acidic (Fig. 1d) and alkaline (Fig. 1e) fuel cells based on the types of electrolytes/membranes used and the charged ions passing through the electrolytes. For the acidic DLFCs, the proton exchange membrane (PEM, for example, Nafion membranes) has been widely used [3]. In the PEM fuel cells, the H⁺ ions pass through the Nafion membrane from anodes to cathodes, receiving electrons to react with O₂ and generating H₂O as the product. As for alkaline DLFCs, anion exchange membranes (AEM) have been developed and widely studied nowadays [22]. In the AEM fuel cells, the OH⁻ ions pass through the AEM and travel to the anodes and react with liquid fuels, generating CO₂ and H₂O as the products. Compared with alkaline DLFCs, acidic DLFCs provide higher current and power density at a relatively lower temperature, however, the main problem is their high dependence on PGMs-based catalysts for both anodes and cathodes [4]. Also, the traveling fuels (such as methanol) from the anodes to the cathodes (i.e., fuel crossover) through the Nafion membrane is a big issue, which not only decreases the fuel cell efficiency but also results in performance decay caused by the mixed potentials at the cathodes. While for the alkaline DLFCs, the less expensive metals, such as nickel (Ni), cobalt (Co), and iron (Fe)based materials, have been developed to replace the PGMs. Thus, the cost of alkaline DLFCs is reduced compared with acidic DLFCs. In addition, the fuel crossover rate is much lower for alkaline DLFCs than acidic ones owing to the reverse transfer of OH⁻ ions from the cathodes to the anodes [72–74]. However, as the main product at the anodes, the generated CO₂ can react with the electrolytes to form carbonates and thus decrease the conductivity of AEM, which reduces the overall cell efficiency, power density, and lifetime. Also, the sluggish redox reactions in the alkaline DLFCs result in a lower power density than the acidic DLFCs. Besides, both acidic and alkaline DLFCs face the CO poisoning issues of PGMs, which should be addressed for commercialization.

Different from H₂-PEMFCs, the main overpotential of DLFCs comes from the anodes due to the sluggish fuel oxidation rate [75]. As shown in the polarization curve (Fig. 1h) [15,16,76], the actual voltage of DLFCs is lower than the ideal/theoretical voltage (Table S1) because of fuel crossover. The cell voltage has a rapid drop induced by activity loss, followed by the liner drop in the ohmic polarization region (the fuel cells operation area for practical application); after that, the mass transport region appears due to high current density. Thus, it is important to maximize the actual voltage of DLFCs, which acquire a higher power density at a lower applied load to enhance the overall cell efficiency.

Some descriptors have been developed to evaluate the activity of DLFCs and anode fuel electrooxidation reactions. The most important one is the peak power density as shown in Fig. 1(h),

which can directly reflect the overall performance of fuel cells. Cyclic voltammetry (CV) has been widely used to assess the activity of the catalysts at the anode in a half-cell. As shown in Fig. 1(i), in the forward scan (taking ethanol oxidation as an example), the ethanol is oxidized on the polycrystalline Pt electrode and shows two typical areas. The first one is the adsorption/desorption regions of hydrogen (H_{ads}) and is usually used to evaluate the electrochemical surface area (ECSA) of the catalysts, which is the direct descriptor to reflect the amount of the exposed active sites. Generally, the higher ECSA, the greater activity for the redox reactions. Then, an electrical double-layer capacitance (C_{DL}) shows up due to the non-Faradaic current. The obvious Faradaic current occurs as the potential increases, which is defined as the onset potential (E_0) . The lower E_0 , the better catalytic capability to drive the ethanol (or other small organic molecular fuels) electrooxidation reactions. The current sharply increases as the potential further increases until reaching the forward peak current (I_f) , which is one of the most important criteria for evaluating the performance of the catalysts. While further increasing the potential, the surface of Pt will be passivated, resulting in the decrease of catalytic activity and thus current drop. During the forward scan, the intermediate species, such as CO, will be adsorbed on the Pt surface, causing CO poisoning. At the backward scan, the passivated Pt will be gradually reduced to a clean Pt surface, and the adsorbed intermediate species on the Pt surface will be further oxidized and result in a backward peak current (I_b) . The lower I_b , the less adsorbed intermediate species on the electrode surface. The value of I_f/I_b is usually used as a descriptor to reflect the anti-poisoning ability of the catalysts [77]. Besides, as CO is the main poisoning species, CO stripping experiments are mainly used to evaluate the property of antipoisoning. The lower CO oxidation potential, the better activity of the catalysts. Also, the CO stripping experiment is a more accurate method to calculate the ECSA compared with Hads, especially for Pd-based materials due to the hydrogen spillover effect [78,79]. Apart from the activity, stability is another important parameter to assess the potential application of a given catalyst, which is genmeasured through multiple-CVs, long-time chronoamperometry/chronopotentiometry.

3. Atomically dispersed catalysts for DLFCs

In the past decades, the most efficient catalysts for electrooxidation reactions of small liquid molecules are noble metals, particularly Pt and Pd NPs. However, the electrooxidation reaction only occurs on the metal surface, the non-accessible metal atoms inside these PGMs NPs are inactive and wasted [80]. It has been reported that the most suitable size of NPs is 3–5 nm [80]. Fortunately, research in the recent decade has proved that the ADCs materials show superior performance compared with the nanoscale materials for small molecular electrooxidation reactions in DLFCs [38.81–83].

3.1. Atomically dispersed catalysts for methanol electrooxidation reaction (MOR)

Direct methanol fuel cells (DMFCs) are one of the most studied DLFCs. Methanol as fuel has a lot of advantages over H₂, such as much higher energy density, relatively cheaper price, and easier handling/transportation/storage. Besides, it can be directly fed into the anodes without any pre-reforming process. However, during the methanol electrooxidation process, the dominant pathway is the indirect process with the formation of CO as an intermediate species [23]. The CO intermediate can easily poison the Pt NPs, which significantly reduces the catalytic activity and stability of MOR catalysts in DMFCs [84]. To alleviate the CO poisoning issue,

a widely used artifice is to add another foreign metal (M, such as Ru, Au, Co, etc.) into Pt to form PtM alloys. Thus, a so-called bifunctional mechanism and electronic effect is generated in PtM, which will facilitate the removal of CO_{ads} from the Pt surface [85–87]. For the bifunctional mechanism in MOR, M provides a much lower potential than Pt to adsorb hydroxyl groups (OH-), which will oxidize the CO_{ads} to the final CO₂. The PtRu is the most representative catalyst for the bifunctional mechanism. While for the electronic effect, the much lower CO adsorption energy on the Pt surface can be achieved due to the modified electronic structure of Pt when alloyed with M, which is beneficial for the oxidation of CO_{ads} on the Pt surface. The strategy of inhibiting CO formation is more straightforward and is much preferred than facilitating CO_{ads} removal to address the CO poisoning issue for MOR [88]. However, the conventionally used nano-catalysts, which were proposed for the CO_{ads} removal, unexpectedly cannot solve the CO poisoning issue completely. Recently, Xing's group reported a series of ADC methods to address this issue thoroughly. First, in contrast to the traditional view, they found that CO can be used as fuel rather than poisoned species on atomically dispersed Rh catalysts (Rh-N-C) in PEMFCs due to the weak CO adsorption on the Rh-N-C [89]. The atomically dispersed IrRu-N-C anode catalyst was further developed for PEMFCs powered with both CO and H₂ [90]. The interplay between Ir and Ru single atom centers synergistic favorably decompose H₂O and further facilitate CO activation. Besides, they also reported a novel catalyst containing both Ir particles and Ir single-atom sites (IrNP@IrSA-N-C) to address the CO poisoning issues [91], where the Ir single-atom sites were recognized as CO oxidizing sites and swept the CO molecules adsorbed on Ir NPs nearby, while the Ir NPs were the active sites for the HOR. Thus, the PEMFCs can be fed with crude hydrogen that contains ppm level CO in anode.

As early as 1981, McNicol has proposed that the MOR needs at least three continuous Pt atoms to act as an active site (Fig. 2a and b) [92]. Thus, the Pt SACs seem powerless for MOR, that is why little work has been reported on SACs for small molecular electrooxidation reactions. In contrast to SACs, the cluster catalysts with continuously bonded Pt atoms can be used as efficient catalysts for MOR. Kim reported a bottom-up single-atom-to-cluster approach (Fig. 2c) to prepare Pt cluster on multiwalled carbon nanotubes (Pth-q/MWNT) and Pt single-atom catalyst on MWNT (Pt-S-MWNT) [93]. The Pt-S-MWNT with Pt single-atoms has no MOR activity due to the absence of Pt-Pt bond. The Pt cluster was formed when the Pt-S-MWNT underwent heat treatment, as a result, an excellent MOR activity was observed (Table 1). Also, the negatively shifted onset potential of MOR achieved in the Pt cluster catalyst was attributed to the modified electronic structure and sufficiently exposed active sites compared with Pt SACs and Pt NPs. And the increased s-d band mixing due to the quantum size effect resulted in the shift of the d-band center. This work suggested that the Pt SACs were not favorable and could not be used as MOR catalysts. Yang et al. prepared Pt supported on titanium nitride (Pt/TiN) with varying Pt loading from 0.35 to 5 wt% [94]. They found that the single-atom Pt mainly existed in 0.35 wt% Pt/TiN, while the 2 wt% Pt/TiN sample showed an intermediate feature, which contained both single-atom Pt and Pt NPs. And Pt NPs were obtained in 5 wt% Pt NP/TiN. Due to the requirement on Pt ensemble sites for MOR, the 0.35 wt% Pt/TiN sample showed barely oxidation current for MOR. And the mass activity for MOR increased with the increasing Pt contents, leading to the highest current density achieved by 5 wt% Pt NP/TiN.

Atomic layer deposition (ALD) technology was also used to develop sub-nanometer Pt cluster catalysts on graphene nanosheets (Fig. 2d) [95]. The Pt size was precisely controlled from the single-atom, sub-nanometer cluster, to NPs with the increased cycle number of ALD. When the ALD was performed for 50, 100,

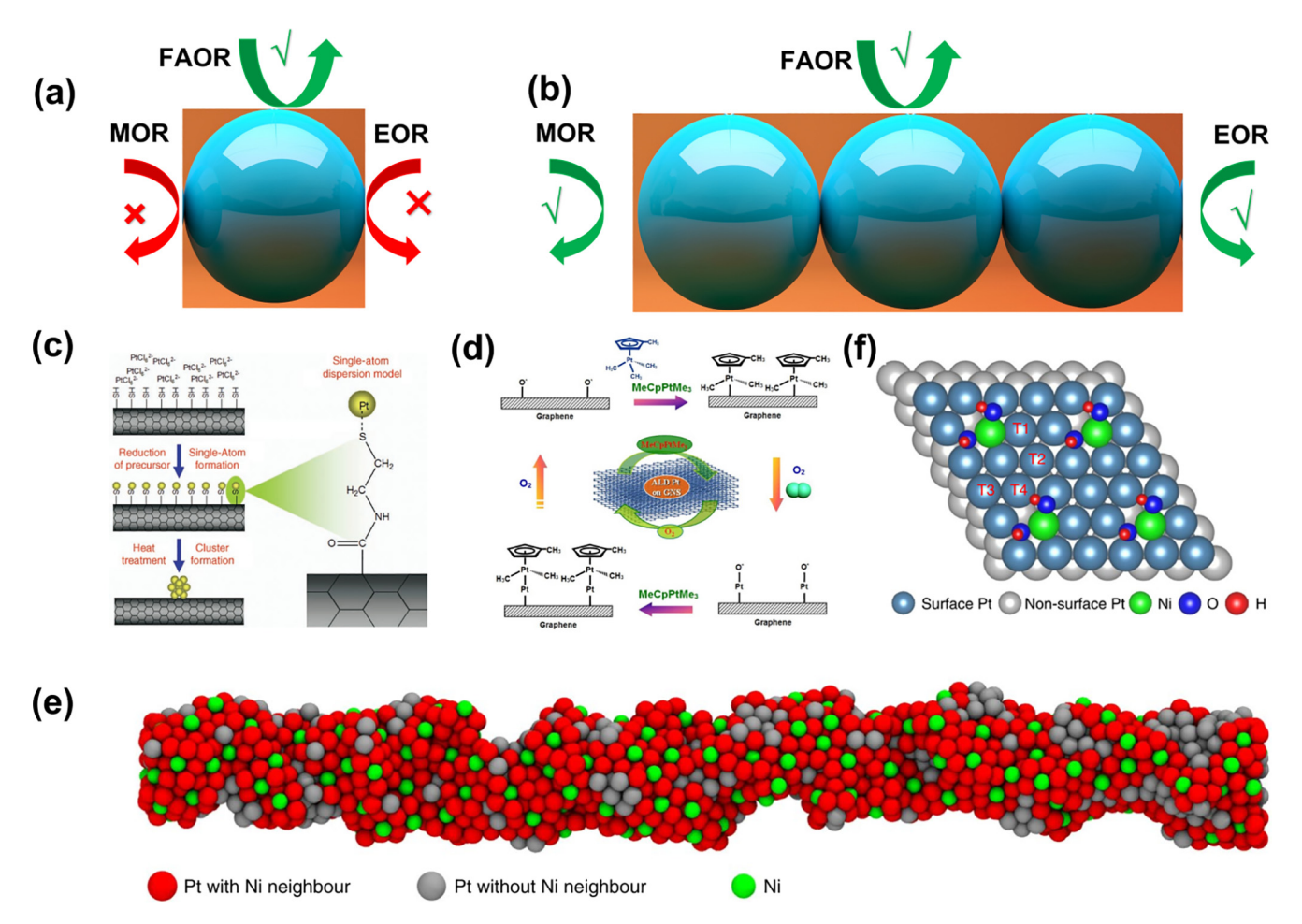


Fig. 2. ADCs for MOR. The activity of (a) a single Pt atom and (b) three contiguous Pt atoms for MOR, EOR, and FAOR. One ball represents one Pt atom. (c) The SACs approach for the preparation of size-controlled Pt clusters. Adapted with permission from Ref. [93]. Copyright 2006 Wiley. (d) Schematic illustrations of Pt ALD mechanism on graphene nanosheets. Adapted with permission from Ref. [95]. Copyright 2013 Springer Nature Group. (e) The schematic diagram for the SANi-PtNWs and (f) model for the SANi-decorated Pt(111) surface with different CO adsorption sites labeled as T1, T2, T3, and T4. Adapted with permission from Ref. [34]. Copyright 2019 Springer Nature Group.

 Table 1

 Representative ADCs for small organic molecules electrooxidations activity in the half-cells.

Fuel	Catalyst ^a	Electrolyte	Current density (A mg $_{PGMs}^{-1}$)	Peak potential (V vs. RHE)	Ref.
Methanol	Pt _{h-q} /MWNT (Th = 523 K)	0.5 M H ₂ SO ₄ with 2.0 M CH ₃ OH	~0.06 A cm ⁻²	0.88	[93]
	ALD50Pt/GNS	0.5 M H ₂ SO ₄ with 1.0 M CH ₃ OH	22.9 mA cm ⁻²	0.79	[95]
	2% Pt/TiN	0.1 M HClO ₄ with 0.5 M CH ₃ OH	0.35	~0.85	[94]
	SANi-PtNWs (106.2 m ² g ⁻¹)	1.0 M KOH with 1.0 M CH ₃ OH	7.93	~0.816	[34]
Ethanol	SANi-PtNWs	1.0 M KOH with 1.0 M C ₂ H ₅ OH	5.60	~0.785	[34]
	Pd CNCs (102 m ² g ⁻¹)	1.0 M KOH with 1.0 M C ₂ H ₅ OH	1.43	~0.8	[112]
	Pd/N&F-C	1.0 M KOH with 1.0 M C ₂ H ₅ OH	26.5	0.87	[56]
	PtBi@PtRh₁	1.0 M KOH with 1.0 M C ₂ H ₅ OH	13.02	~0.98	[115]
	PdZn/NC@ZnO	1.0 M KOH with 1.0 M C ₂ H ₅ OH	18.14	~0.85	[119]
	Au@Ag _{ML} @Pd NWs	0.1 M KOH with 0.1 M C ₂ H ₅ OH	0.64	~0.9	[113]
Formic acid	2Pt/TiN	0.1 M HClO ₄ with 0.5 M HCOOH	1.4	\sim 0.68	[94]
	0.35% Pt/TiN		0.7	\sim 0.72	
	0.05ML Pt on Au Nano-Octahedra	0.1 M H ₂ SO ₄ with 0.5 M HCOOH	62.6	0.52	[98]
	Pt ₁ Au ₂₄ cluster	0.1 M HClO ₄ with 0.5 M HCOOH	3.7	\sim 0.6	[123]
	Pt ₁ /ATO	0.1 M HClO ₄ with 0.5 M HCOOH	3.35	\sim 0.6	[97]
	Pt ₄ Au ₉₆	0.1 M HClO ₄ with 0.1 M HCOOH	3.77	\sim 0.6	[122]
	Ir ₁ /CN	0.5 M H ₂ SO ₄ with 0.5 M HCOOH	12.9	0.7	[124]
	Rh ₁ /CN	0.5 M H ₂ SO ₄ with 0.5 M HCOOH	16.1	0.7	[125]

^a Due to the loss of metal character, the ECSA for most ADCs cannot be detected and no given.

and 150 cycles, the corresponding Pt sizes were reported to be 0.5 nm, 1–2 nm, and 2–4 nm with a Pt loading of 1.52, 2.67, and 10.5 wt% on graphene, respectively. These ALD prepared samples

demonstrated enhanced performance than benchmarking Pt/C for MOR. However, the onset potentials for MOR positively shifted as the ALD-cycles number increased, so did the peak potentials. With

50 ALD cycles, Pt/GNS showed the best MOR performance. The negative shifts of both the onset and peak potentials of the ALD Pt/GNS catalysts indicated significantly reduced overpotentials for MOR than commonly used Pt/C catalyst. For the MOR activity, the current density of 50 ALD Pt/GNS (22.9 mA cm⁻²) showed 9.5 times higher than that of Pt/C catalyst (2.41 mA cm⁻², Table 1). The intrinsic nature of sub-nanometer Pt clusters and the existence of oxygen-containing functional groups on graphene nanosheets were the main reasons for the enhanced MOR activity.

When designing a catalyst for MOR, the CO poisoning issue should be considered because of the strong adsorption of poisonous CO intermediate on the Pt surface. Apart from the Pt cluster catalyst for MOR, the single-atom-alloy shows much better performance due to the bifunctional mechanism and electronic effect. Liu et al. reported that the PtCu (1:125) single-atom-alloy could reduce the binding strength between CO and Pt attributed from the single Pt atom [96]. It has been predicted that the single-atom-alloy should have excellent performance for MOR. However, when Pt single-atoms alloyed with Sn [97] and Au [98], they showed no apparent current for MOR due to the insufficient ensemble size to drive the MOR in the presence of CO intermediates [99].

It seems that the single Pt atom and the single Pt atom alloyed with other metals are inactive for MOR. Also, it should be noted that when transition metals were used to decorate Pt, some surface-active sites of Pt would be inevitably blocked, which further resulted in a decreased ECSA (more than 30%-50% lower than the initial ones without modification) [100]. Conversely thinking, we can prepare another type of single-atom-alloy, in which the above-mentioned decorated transition metals may serve as single-atoms surrounded by Pt sites at the nanoscale. In this way, the minimized size of the decorated metal sites will not block the surface Pt sites, while the activated Pt sites with adjacent transition metal atoms will remain at an ensemble size. For example, Li reported single-Ni-atom-modified Pt nanowires using a partial electrochemical dealloying approach (Fig. 2e) [34]. The minimum amount of single Ni atoms was used for decoration, while most surface Pt sites were activated by single Ni atoms, which not only ensured the maximal utilization of Pt but also avoided blocking the active site. The resulting SANi-PtNWs showed a high ECSA of 106. $2 \pm 4.5 \text{ m}^2 \text{ g}_{Pt}^{-1}$ and a high atom utilization of Pt. As a result, such SANi-PtNWs showed a mass activity of 7.93 \pm 0.45 A mg_{Pt}⁻¹ for MOR (Table 1), which was about seven times higher than commercial Pt/ C and two times higher than other catalysts. In addition, the onset potential for MOR was reduced, indicating the lower activation barrier for MOR on the SANi-PtNWs surface than other control samples. The DFT calculation (Fig. 2f) suggested that the adsorption energy of the CO intermediate was 0.06-0.28 eV weaker on the SANi-modified Pt top sites than that on the Pt (111) top sites.

Through DFT calculations, Tran et al. found that the single-ion species of Pt2+ and Pt4+ did not have any catalytic activities and could not promote MOR by themselves [101]. The main reason is that methanol cannot bind to the surface of these cationic sites. Instead, they found that the sub-nanometer metallic Pt (Pt⁰) particles supported on the ceria surface could catalyze MOR. Also, the surface hydroxyl groups near the supported metal NPs facilitated the formation of formaldehyde and product desorption, thus, promoting the MOR. However, most single atom has a strong electronic effect with support or coordinate heteroatoms, forming positively charged single atom (M^{n+}) in the SACs [49,53], which is not beneficial for MOR. Another study from Marcinkowski suggested that the methanol primarily desorbed with a small amount of formaldehyde produced at 516 K on the Pd-free surface of Fe₃O₄ (001) [102]. While the barrier became lower to produce formaldehyde when single Pd atoms presented on the surface of Fe₃O₄ (001). However, in the presence of methoxy intermediates, the

Pd atoms were unstable above room temperature. Thus, the overall yield of formaldehyde and the low-temperature pathway is largely inhibited by the Pd sintering, which is a serious stability concern for SACs.

From the discussion above, it seems that the Pt (or other PGMs) should be in the forms of single-atom-alloy, cluster, sub-nanoscale, and nanoscale rather than the single-atom for MOR. Very few studies on the single-atom or other types of ADCs were reported for MOR [103]. With the rapid development of advanced characterization techniques, a more insightful understanding of MOR at the molecular/atom level will be achieved in the future.

3.2. Atomically dispersed catalysts for ethanol electrooxidation reaction (EOR)

Direct ethanol fuel cells (DEFCs) should receive more attention than DMFCs since ethanol has a higher energy density than methanol (Fig. 1a and Table S1), along with the nature of non-toxic, noncorrosiveness, easy acquirement from biomass and agriculture products. Besides, compared with methanol, ethanol has a larger molecular size, which results in a lower permeability rate across the membrane than methanol [104]. However, the complete oxidation of ethanol is difficult due to the strong C-C bonds, which consume more energy for complete cleavage and significantly reduce the reaction efficiency. Increasing the temperature seems to be an efficient approach for improving EOR, however, the polymer electrolyte membrane will be dehydrated at high temperatures [105], which causes performance decay. Even though the 12electron pathway of EOR to produce carbon dioxide (CO₂) is the ideal process, there are a lot of by-products generated during EOR, such as acetic acid (or acetate in alkaline) with a 4-electron pathway, or acetaldehyde with a 2-electron pathway, which further lowers the overall performance of DEFCs [106,107]. These drawbacks result in the lower power density of DEFCs than DMFCs [108]. Thus, the ideal EOR catalyst should not only have a good anti-poisoning ability for CO but also can promote the cleavage of C-C bonds at low potential during EOR.

The EOR mechanism is more complex than MOR due to the different adsorbed intermediates [5,104]. From the aspects of electrocatalysis, seeking new catalysts with high activity and good selectivity to promote the cleavage of C–C bonds with a complete 12-electron pathway is crucial for EOR. Same to MOR, Pt and Pd are still recognized as the best catalysts. Recent studies also suggested Pt-based alloys as good candidates due to the bifunctional mechanism. Zhou et al. found that PtSn alloys showed excellent DEFCs performance because of the expanded lattice of PtSn/C catalyst, which was favorable for the cleavage of C–C bonds [109]. While the CO_{ads} intermediates as a result of breaking the C–C bonds could be easily removed by reacting with surface oxygencontaining species. Further gas chromatography (GC) test indicated that the Pt-Sn oxidized ethanol completely, leading to higher ethanol utilization coefficient and fuel efficiency [110].

Same as MOR, at least three continuous catalytic sites are required for initiating EOR (Fig. 2a and b). For example, Weber deposited different Pt atoms on ITO (Pt_n/ITO, where n=1-14) [111]. They found that the isolated Pt atoms had no catalytic activity for EOR, while the Pt₄/ITO and Pt₁₀/ITO with continuous Pt sites showed the best EOR performance. They proposed that the EOR activity was uncorrelated with the Pt 4d binding. The cluster [81] or single-atom-alloy [96] catalysts could be good candidates. However, very few studies on these types of catalysts for EOR have been reported till now [34,112,113]. As we discussed in Section 3.1, besides the good MOR performance, the single Ni atom modified Pt nanowires (SANi-PtNWs) also showed outstanding EOR performance. The SANi-PtNWs showed a peak mass activity of 5.60 \pm 0. 27 A mg_{Pt}⁻¹ at 0.785 V (Table 1), which was about seven times

higher than Pt/C and three times higher than pure-PtNWs. In addition, the EOR onset overpotential for the SANi-PtNWs was reduced compared with Pt/C, indicating that the ethanol was much easier to be oxidized on the SANi-PtNWs. The weaker CO adsorption on the SANi-modified Pt sites than that on the Pt (111) sites was responsible for the enhanced EOR performance (Fig. 2f).

Kowal reported ternary Pt/Rh/SnO2 electrocatalysts for completely oxidizing ethanol to CO₂ at room temperature [114]. They found that the water molecules strongly adsorbed on the SnO2 sites, suffering the spontaneous O-H bonds breakage (Fig. 3a). In contrast, both Pt and Rh sites are much less active than SnO₂, and the water molecules stay intact on these sites. Thus, the SnO₂ sites are occupied by H₂O/OH during the electrochemical process (Fig. 3b). The weaker interaction between H₂O and Pt/Rh was observed, making them available for ethanol oxidation due to the low-coordination sites of Pt/Rh. For the C-C bond cleavage on the Pt/Rh/SnO₂, the pathway (i.e., *CH₂CH₂OH \rightarrow *CH₂CH₂O + H* \rightarrow *CH₂ $CH_2O + 2H^* \rightarrow {^*CH_2} + {^*CH_2}O + 2H^*$) seems optimal. All the adsorbates prefer to be adsorbed on the pure Rh sites except atomic H, which makes the Rh-Pt hybrid hollow and clean sites, and the barrier to CH₂CH₂O generation decreases in the following sequence as $Pt/SnO_2 > Rh/SnO_2 > PtRh/SnO_2$. Thus, the Rh sites are necessary for the formation of *CH₂CH₂O. Besides, the Rh and Pt compound facilitates the appearance of more empty states of Rh than Rh alone does on SnO₂. An electron transfer from Rh to Pt results in a strong interaction between Pt and Rh, which further creates more available d-states of Rh above the Fermi level (Fig. 3c). Meanwhile, the d-states of Pt shifts away from the Fermi level, resulting in a lower activity of Pt than Rh in the PtRh/SnO₂, so does the activity of Pt in the Pt/SnO₂. Thus, the weak interaction between Pt in the PtRh/SnO₂ and ethanol, as well as other dissociated oxygenates and hydrocarbons can be formed. All these synergistic effects simultaneously contribute to a high EOR activity on the Pt/Rh/SnO₂.

Recently, Luo et al. reported a tensile-strained Pt–Rh single-atom alloy (PtBi@PtRh_1) via electrochemical dealloying from the isolated Rh atoms on ordered PtBi nanoplates (Fig. 3d) [115]. Benefiting from the single atom of Rh_1-tailored Pt (110) surface with tensile strain, the PtBi@PtRh_1 nanoplates show record mass activities of 5.417 A mg_1+Rh at 0.6 V and 13.02 A mg_1+Rh at the peak potential (Fig. 3e, left). They found that the synergy between the tensile strain effect by forming PtBi core–Pt shell and the electronic effect by dispersing Rh as single atoms was the main reason to boost the EOR. In addition, they also found that the PtBi@PtRh_1 nanoplates exhibited enhanced possible C1-pathway selectivity in comparison with PtBi@Pt nanoplates and Pt/C (Fig. 3e, right),

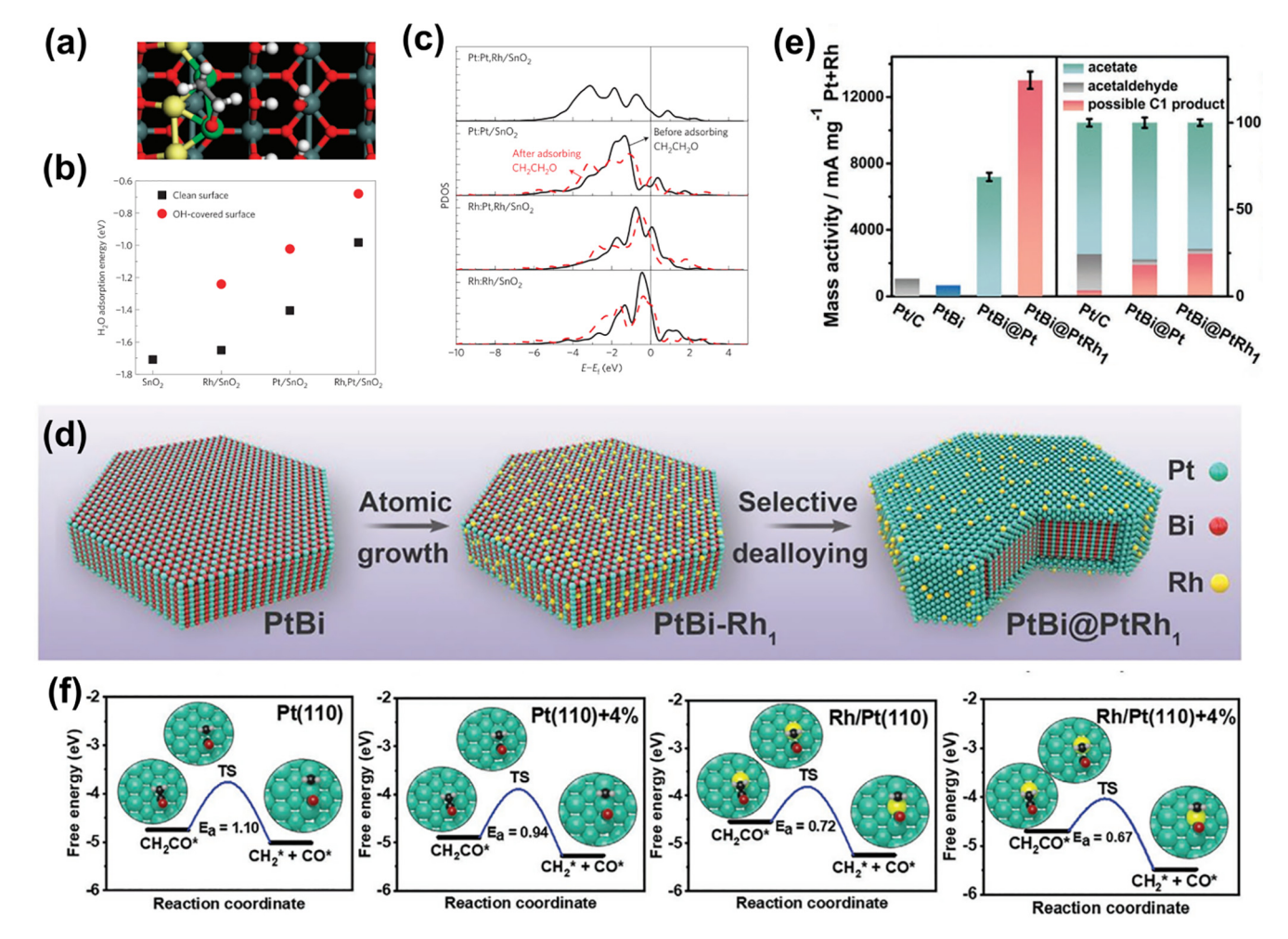


Fig. 3. Pt-based ADCs for EOR. (a) Optimized geometry of CH₂CH₂O adsorption on RhPt/SnO₂(110) surface. (b) DFT-calculated adsorption energies of water on the surfaces of SnO₂(110), Rh/SnO₂(110), Pt/SnO₂(110), and RhPt/SnO₂(110) with and without water saturating the SnO₂ sites. (c) Calculated PDOS of the d-state of Pt or Rh on the Rh/SnO₂(110), Pt/SnO₂(110), and RhPt/SnO₂(110) surfaces. Adapted with permission from Ref. [114]. Copyright 2009, Springer Nature Group. (d) Schematic illustration of the preparation procedure of and PtBi@PtRh₁ annoplates. (e) Noble-metal mass-normalized activity and selectivity of PtBi@PtRh₁ and control catalysts. (f) Energy profiles for breaking the C–C bond of the CH₂CO intermediate on different samples. The green, yellow, red, black, and grey spheres represent Pt, Rh, O, C, and H, respectively. Adapted with permission from Ref. [115]. Copyright 2021 Wiley.

thus verifying that both single-atom Rh tailoring and tensile-strained Pt are effective in facilitating the cleavage of the C-C bonds during EOR. From the DFT calculations, it is found that the Rh doping into the Pt (110) and tensile strain will modify the d-states of catalytic surface and upshift the d-band center closer to the Fermi level, resulting in the stronger adsorption of ethanol and lowering the activation barriers of C-C bonds breaking (Fig. 3f). Thus, the construction of a single-atom alloy will be an efficient strategy for the future research of electrocatalysts for MOR and EOR due to the prerequisites of ensemble effect.

It is reported that the Pd-based catalyst has higher catalytic activity and better steady-state performance for EOR than Pt in alkaline media [116,117]. Recently studies also indicated that the catalytic activity of ADCs was largely dependent on atomic geometry. Liu et al. precisely controlled the atomic geometry of Pd shell atoms on the Au nanowires [113]. Through this method, the isolated and continuous Pd atoms supported on the surface of Au nanowires were obtained and studied (Fig. 4a). Due to the weak interaction between the Pd atoms and the Au supports, the Pd atom ensembles rather than forms isolated Pd single-atoms on the Au surface. On the contrary, coating Ag monolayers (ML) to form Au@Ag_{MI} core-shell nanostructures was an efficient approach to prepare Au@Ag_{MI}@Pd nanowires with single Pd atoms. The electrocatalytic EOR activity was largely dependent on the geometry of Pd atoms. As shown in Fig. 4(b), the Au@Pd structures with different sub-monolayers showed four times higher mass activity for EOR than that of Pd/C. Also, the EOR activity on the Au@Ag_{ML}@Pd nanowires was largely dependent on the Pd coverage, where a Pd coverage of 1/16 to 1/4 monolayer (ML) was almost electrocatalytically inert for EOR. When the Pd coverage was 1/2 ML and 1.0 ML, the mass activity for EOR reached 0.16 and 0.35 A mg_{Pd}^{-1} , respectively. Furthermore, the relative amount of continuous Pd atoms determined the EOR activity of Au@Pd and Au@AgML@Pd nanowires (Fig. 4c). It is convinced that the single Pd atom is inert for EOR while the Pd ensembles are the active sites for EOR.

The local coordination environment around catalytically metal active sites also plays a vital role in EOR. Recently, Yang's group reported that introducing F atoms into Pd/N-C catalysts could modify the environment around the Pd (Pd/N&F-C, Fig. 4d) and improve activity, selectivity, and durability for EOR. They found that N-rich Pd surface was created after F introduction, thus local coordination environment of Pd was tuned. The surface riched Pd-N formed on Pd inhibits the mobility and aggregation of Pd NPs and avoids electrochemical Ostwald ripening, thus showing much higher EOR activity and stability (Fig. 4e and Table 1). It is also found that the selectivity from EOR to CO₂ through a C1-12e pathway was dramatically increased on the Pd/N&F-C compared with the control samples (Fig. 4f). When employed as anode and cathode catalysts using Pd/N&F-C, the maximum power density was as high as 0.57 W cm⁻² (Fig. 4g), several folds higher than the sample without F doping, commercial Pd/C, and Pt/C. The more important thing is that the DEFC device can be continuously operated for more than 5900 h at a high output power density without obvious performance decay. In addition, they also proved that the EOR performance of Pd/C catalysts containing other heteroatoms (P, S, B) can also be improved through the addition of F atoms (Fig. 4e). This work not only provided a potential way to increase the catalytic activity and selectivity for EOR but also may resolve the corrosion issue of carbon materials used in various related electrochemical energy devices.

Apart from the catalytic metals used, the functional support materials and the metal-support interface also play a vital role in the catalytic reaction [118]. For example, N-doped carbon-coated ZnO (NC@ZnO) support was developed by the Li group [119]. The Pd-Zn dual sites on NC@ZnO were obtained (PdZn/NC@ZnO) due to that the Zn evaporates easily at high temperatures during Pd

loading. Comparing $Pd_n/NC@ZnO$ with Pd-Pd sites to $Pd_1/NC@ZnO$ with individual Pd sites, the PdZn/NC@ZnO with Pd-Zn dual sites makes for the adsorption of ethanol and OH^- much easier, thus displaying much higher activity and stability for EOR (18.14 A mg_{rd}^{-1} , or 54.60 mA cm⁻², Table 1) in 1 M ethanol containing 1 M KOH solution. Hence, using suitable support to create strong metal-support interactions and further constructing dual sites also can promote the EOR performance.

Ding et al. [112] found that the Pd colloidal nanocrystal clusters (CNCs) showed a much better EOR activity than Pd NPs, due to the smaller size of Pd CNCs (\sim 10 nm vs. \sim 35 nm Pd NPs). The Pd CNCs exhibited a two-times higher specific current density of 1.43 A mg⁻¹ than that of Pd NPs (Table 1). Besides, the onset potential of Pd CNCs for EOR negatively shifted compared with Pd NPs. However, when the current was normalized to the real surface area of Pd. the Pd CNCs showed an inferior activity than Pd NPs because of the much lower ECSA of Pd NPs. Thus, it is important to enhance the electrocatalytic activity from the perspectives of mass activity (maximum utilization of per atom) and specific activity (maximum utilization of per active site) simultaneously. The oxidation of other small organic alcohol fuels on the Pd CNCs and Pd NPs were also compared, and the electrocatalytic activity followed the order of ethanol > glycol > methanol > propanol > isopropanol on the Pd NPs and Pd CNCs electrodes [112]. The onset potential for EOR was much more negative than other studied alcohols, due to the difficulty in splitting the strong C–C bonds in the C_{3+} alcohols.

3.3. Atomically dispersed catalysts for formic acid electrooxidation reaction (FAOR)

Direct formic acid fuel cells (DFAFCs) show much more advantages over DMFCs and DEFCs, including lower toxic and ecofriendly nature, higher open-circuit voltage (1.48 V vs. 1.21 V with methanol and 1.14 V with ethanol, Fig. 1b and Table S1), faster oxidation kinetics, as well as lower crossover rate through Nafion membrane. Besides, the high concentration of formic acid can be directly used in the anodes without adding other acidic additives to increase the ionic conductivity. More importantly, only a 2-electron transfer process is needed for complete electrooxidation of formic acid, which is dynamically easier than MOR (6-electron process) and EOR (12-electron process, Fig. 1c).

The oxidation of formic acid is generally recognized to proceed through two pathways, namely the direct pathway (dehydrogenation) and indirect pathway (dehydration), as shown in Fig. 5(a). The direct pathway is more favorable because no CO is generated during this process, which means that the surface of catalysts remains clean without CO poisoning. Moreover, it is widely accepted that Pd is much more active for FAOR than Pt because Pd prefers the direct pathway while Pt tends towards the indirect pathway [120]. Thus, the most reported nanoscale catalyst was Pd-based materials rather than Pt-based ones (Tables S2 and S3). While the ADCs for FAOR focused on Pt. The DFT calculation performed by Neurock et al. [121] suggested that only 1-2 Pt atoms were needed to activate O-H bonds for the direct pathway; while Pt ensemble sites were required to activate C-O bonds for the indirect pathway (Fig. 5a). Thus, single-atom Pt (or other single-atom catalysts) will follow the direct pathway for FAOR due to the absence of Pt ensemble sites, which is different from the required ensemble sites for MOR and EOR. In theory, the SACs should have superior FAOR activities than traditional nano-catalysts due to the increased number of active centers to proceed through the direct pathway. Recently, a singleatom-alloy of Pt₄Au₉₆ for FAOR was reported [122]. The results indicated that the local bonding environment of single-atomic-site Pt surface atom played the main role in boosting the activity. The CO adsorption on Pt (111) was weakened on the single-atom Pt surfaces compared with the bulk Pt (Fig. 5b and c). In addition, only one Pt

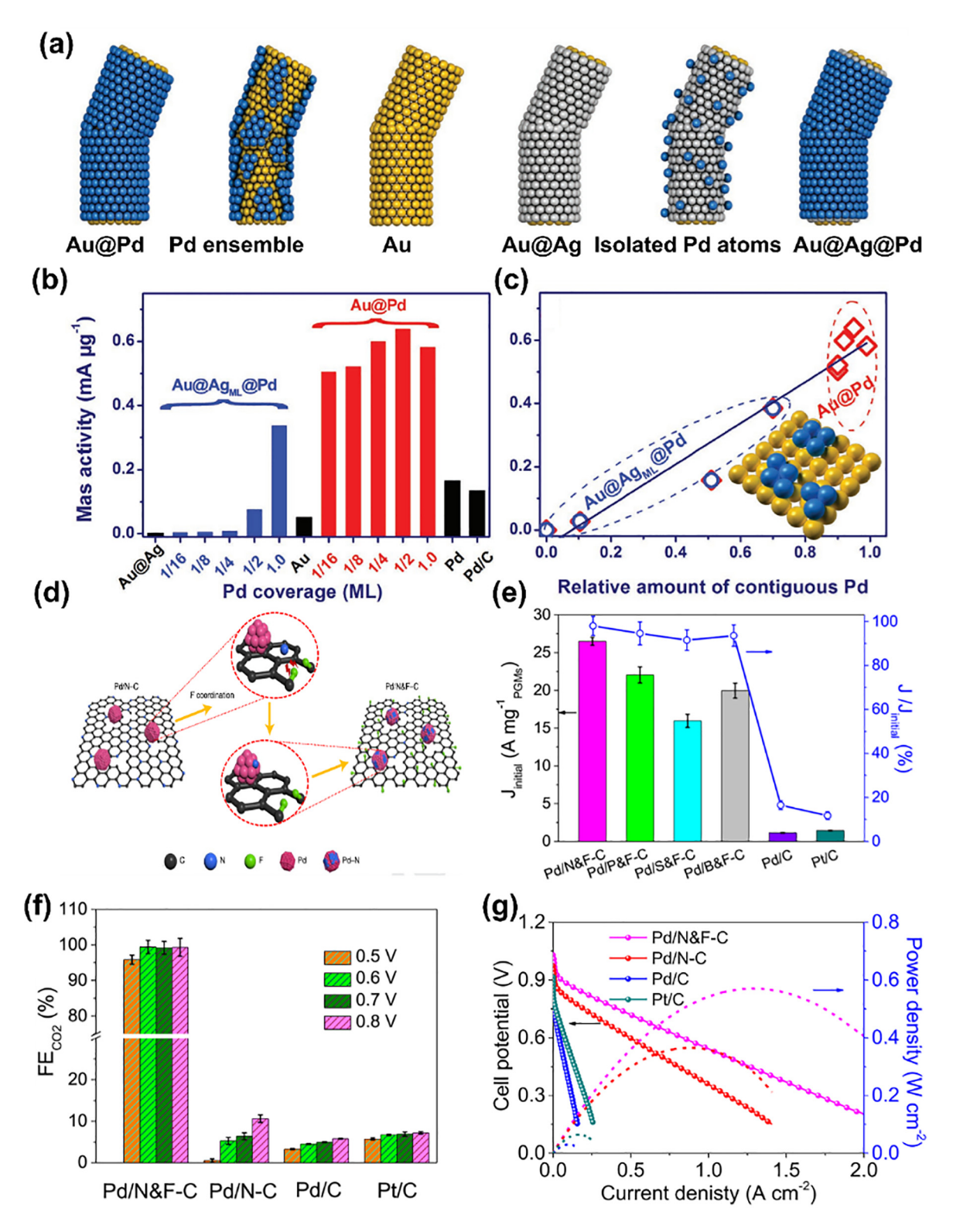


Fig. 4. Pd-based ADCs for EOR. (a) Schematic illustration of tailoring the atomic geometry of Pd atoms on the Au NW surface using an Ag ML. (b) Electrocatalytic performance of Au@Pd and Au@Ag_{ML}@Pd nanowires with different Pd coverages in 0.1 M KOH + 0.1 M ethanol. (c) The relationship between EOR activity and the relative amount of Pd ensembles. Adapted with permission from Ref. [113]. Copyright 2017, Wiley-VCH. (d) Schematic illustration of the fluorination-driven rearrangement of the LCE on Pd/N-C. (e) EOR MA (left axis) and the corresponding retention (right axis) after 10000 cycles of different samples. (f) Faradaic efficiency of ethanol to CO₂ on different samples in a half-cell. (g) Steady-state DEFC polarization and power density curves of different samples. Adapted with permission from Ref. [56]. Copyright 2021, Springer Nature Group.

adsorption site is required for formic acid dehydrogenation, whereas the indirect dehydration pathway requires a greater number of adjacent atoms. Thus, the direct dehydrogenation reaction is

the primary reaction pathway on the isolated single-atom catalytic sites of Pt₄Au₉₆, which shows more CO-tolerance and results in a high FAOR activity (Fig. 5d and e and Table 1).

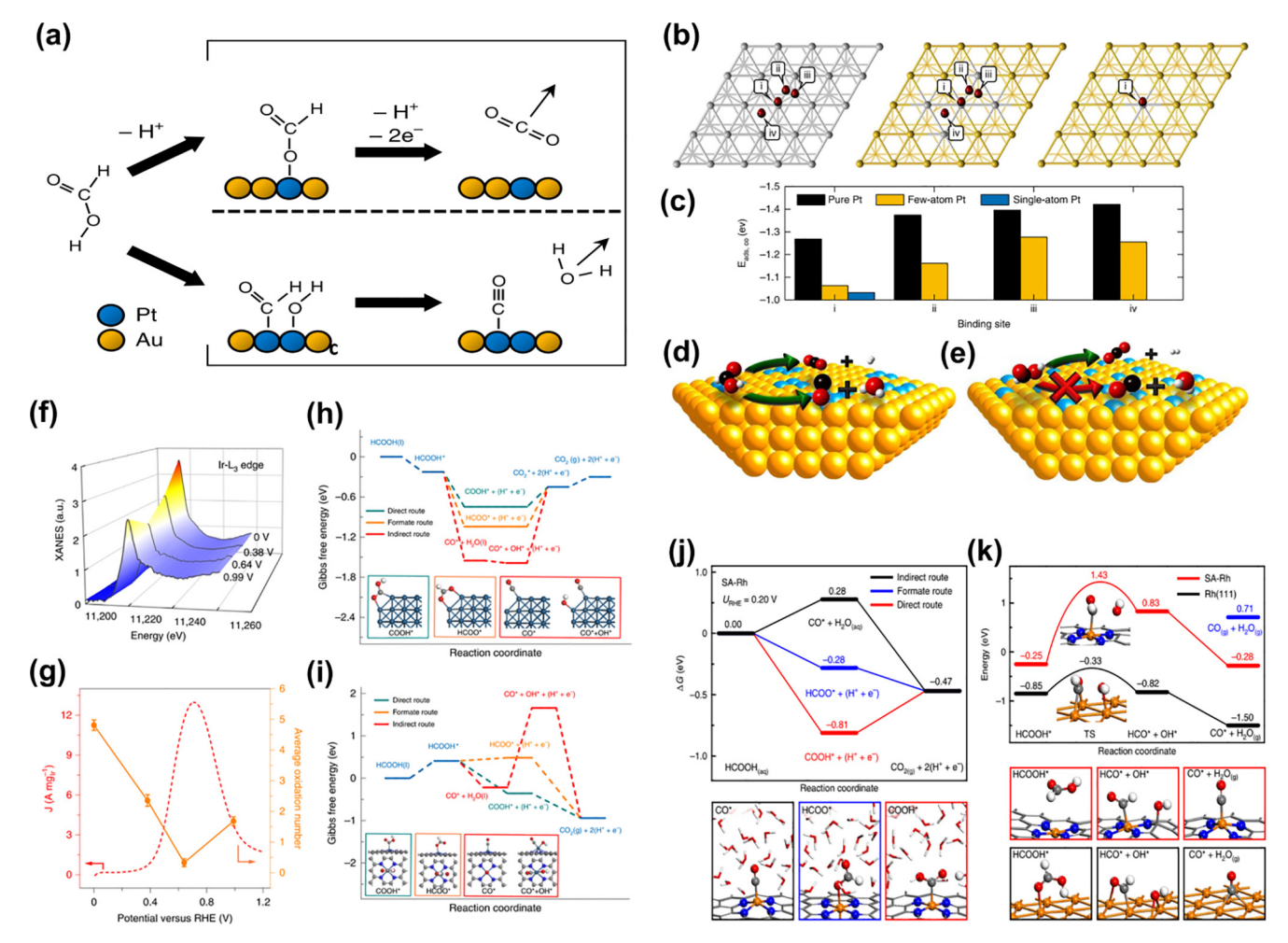


Fig. 5. ADCs for FAOR. (a) Illustration of the dehydrogenation (top) and dehydration (bottom) mechanisms of the FAOR reactions. (b) Illustration of CO adsorption modes on model (111) lattices of pure, few-atom, and single-atom (from left to right) Pt surfaces that shows the apical (i), bridging (ii), hexagonal close-packed hollow (iii), and face-centered cubic hollow (iv) coordination sites. (c) Calculated adsorption energies for the indicated CO adsorption sites. Predominant FAO reaction pathways on (d) few-atom (or greater) and (e) single-atom Pt surfaces, which highlights the selectivity achieved via the ensemble effect. Spheres: Au, yellow; C, black; H, white; O, red, Pt, blue. Adapted with permission from Ref. [122]. Copyright 2018 Springer Nature Group. (f) Iridium L₃-edge XANES spectra of Ir₁/CN at various potentials during the potentiostatic FAOR. (g) The current density as a function of potential for Ir₁/CN (left) and the average oxidation numbers of iridium in Ir₁/CN as a function of potential (right). A Gibbs free energy diagram of the FAOR on (h) Ir/C and (i) Ir₁/CN. Adapted with permission from Ref. [124]. Copyright 2020 Springer Nature Group. DFT calculation on (j) free energy profiles of formic acid oxidation via indirect, formate, and direct routes on the SA-Rh site. Bottom: optimized structures of the intermediates in the three routes. (k) potential energy profiles of formic acid decomposition to CO on the SA-Rh site (red curve) and the Rh (111) surface (black curve). Bottom: corresponding structures of the intermediates and transition states (TSs). White, grey, blue, red, and orange balls represent H, C, N, O, and Rh atoms, respectively. Adapted with permission from Ref. [125]. Copyright 2020 Springer Nature Group.

Some other experimental studies have also proven the abovementioned conclusions achieved by DFT calculations. For example, the atomically dispersed Pt single-atom catalyst on Au octahedra was used for FAOR. The atomic Pt (0.05 ML Pt) showed two times higher activity than Pt/C for FAOR due to the direct pathway of FAOR on the Pt SACs [98]. When comparing the modified electronic structure, it seems that the bare gold surface is more important in the Pt-Au system to facilitate the direct pathway. Lu et al. [123] combined the Pt single-atom with Au cluster (Pt₁Au₂₄), the mass activity of which (3.7 A mg_{Pt+Au}^{-1}) was about 12 times greater than the Pt nanoclusters and 34 times higher than Pt/C catalyst, respectively. Besides, the Pt SACs supported on TiN (2% Pt/TiN) also showed considerable FAOR activity with a peak current density of 1.5 A mg_{Pt}⁻¹ following a direct pathway [94]. While this current density is still lower than the above-mentioned 0.05 ML Pt on Au, mainly due to the different metallic states of the catalysts, where the Pt in Pt/TiN is quite oxygenated, while the Pt in 0.05 ML Pt on Au is metallic. Besides, the single-atom Pt catalyst supported on Sb-doped SiO₂ (Pt₁/ATO) was also used for FAOR [97],

which showed ca. 20 times higher activity on 4 wt% Pt₁/ATO than commercial Pt/C. The catalytic process on Pt₁/ATO is via a direct pathway without CO poisoning. The DFAFCs using Pt₁/ATO as the anode catalyst showed a similar power density (\sim 35 mW cm⁻²) to that of commercial Pt/C, though only 1/10 of the amount of Pt was used. This proves that minimizing Pt content while remaining the same power density can be achieved through the maximum utilization of PGMs.

Previous studies [124] indicated that many metallic SACs (such as Ru, Mo, Ga, Cu, Ni, and Mn) showed no activity for FAOR. On the contrary, Ir SAC (Ir₁/CN) was extremely active for FAOR [124]. The *in-situ* XAFS study indicated that the average oxidation number of Ir decreased as the applied potential increased from 0 to 0.64 V (Fig. 5f). The average oxidation number of Ir strongly relied on the applied potential and current density for FAOR (Fig. 5g), where it decreased with increasing the current density. This trend suggests that the atomically dispersed Ir species are the active centers for FAOR, whose 5*d* band occupancy becomes higher because of electron transfer from formic acid to Ir. Furthermore, from the

DFT calculation, it is found that Ir/C NPs had an indirect pathway (Fig. 5h) for FAOR due to the strong binding of CO* on the Ir/C surface than COOH* and HCOO*. Both CO* and OH* are thermodynamically stable on the Ir/C due to the existence of the Ir-Ir bonds, while the CO* needs much higher energy input to be oxidized to CO_2 . The generated CO_2 at higher potential further adsorbed on Ir/C and blocked the Ir active sites. In all, the CO poisoning and the occupied CO₂ on the Ir/C surface result in a poor FAOR performance. In contrast, the d-orbital vacancy was larger for Ir-N₄ (active site in Ir₁/CN), resulting in a weaker bonding of Ir-N₄ and CO (Fig. 5i). When catalyzing formic acid electrooxidation on the Ir_1 / CN, the cleavage of the C-H bonds is an exothermic process, which is much more favorable than the formation of CO*. Thus, a high activity of FAOR without the formation of poisonous CO on the Ir₁/CN was obtained through a direct pathway. Apart from Ir₁/CN ADCs, single-atom Rh dispersed on N-doped carbon (SA-Rh/CN) was also found to be an efficient catalyst for FAOR [125]. The cleavage of C-O bonds in HCOOH was difficult on the SA-Rh site (Fig. 5j), while a formate route without CO generation was preferred on the SA-Rh/CN during FAOR. Also, compared with Rh (111), the downward shift of the d-orbital below the Fermi level and the much lower the density of state (DOS) at the Fermi level were found on the SA-Rh/CN (Fig. 5k). As a result, the adsorption of SA-Rh was much weaker than that on the Rh (111). The adsorption energy of CO at the SA-Pd and SA-Pt sites was both too weak, while much higher adsorption energy of CO was found on Rh(111) surface. Thus, only the Rh/CN has a suitable binding ability with intermediates, which results in startling catalytic activity for FAOR (Table 1).

3.4. Fuel cells performance of ADCs

Even though the ADCs show great advantages over nanoscale catalysts, few studies are reporting the real device performance based on ADCs because of the newly emerging concept of ADCs or single-atom catalysts [53]. Fig. 6(a-c) illustrates the representative performance of DMFCs, DEFCs, and DFAFCs. The maximum power density of DLFCs still cannot catch up with the performance of H_2 -PEMFCs (single-cell performance of >1 W cm⁻²) due to their much slower reaction kinetics of liquid fuel oxidation than HOR at

the anodes. In addition, the current technology is still incapable of matching the U.S. Department of Energy (DOE) target due to the high PGMs loading to ensure sufficient power density and stability [126]. Thus, it is critical to reduce the usage amount of PGMs and maximize the atom-utilization to push the DLFCs commercialization. Apart from the activity, stability is another important parameter that determines the lifetime of fuel cells to meet the application expectations. The present technology is still far away from the DOE target even with the best catalysts. The stability of all reported DLFCs can only be maintained for hundreds of hours (Fig. 6d), which is much shorter than the DOE target which asks at least 40000 and 5000 h for stationary and transportation fuel cells, respectively, under realistic operating conditions [126]. Recently, Yang's group reported an effective F doping method which not only increases the activity of DEFCs but also stably operates at high power density for more than 5900 h [56], which is a big breakthrough in the fuel cell developments and will stimulate other researchers to explore similar materials in fuel cell community. Besides, significant efforts should be paid not only to lower the usage of PGMs but also to keep the catalytic activities for a long enough time. As the present catalysts based on nano-scale strategy show slow development for the fuel cells, the ADCs strategies, which can maximize the PGMs utilization and significantly decrease the loading of PGMs, have been the recent research focus [45,46,48,58].

5. Summary and outlook

DLFCs have shown great promises as clean energy solutions to the energy crisis and environmental concerns. In this review, the performance of DLFCs from fundamental to practice performance was summarized. Much more attention should be paid to the anode electrooxidation reaction for DLFCs due to the sluggish reaction kinetics for carbon-containing fuel electrooxidation. Moreover, the ADCs as the anode catalysts for fuel cells reactions demonstrate unique enhancements in the activity, stability, selectivity, and utilization efficiency of PGMs than the widely studied nano-catalysts. The SACs can be used for FAOR due to the

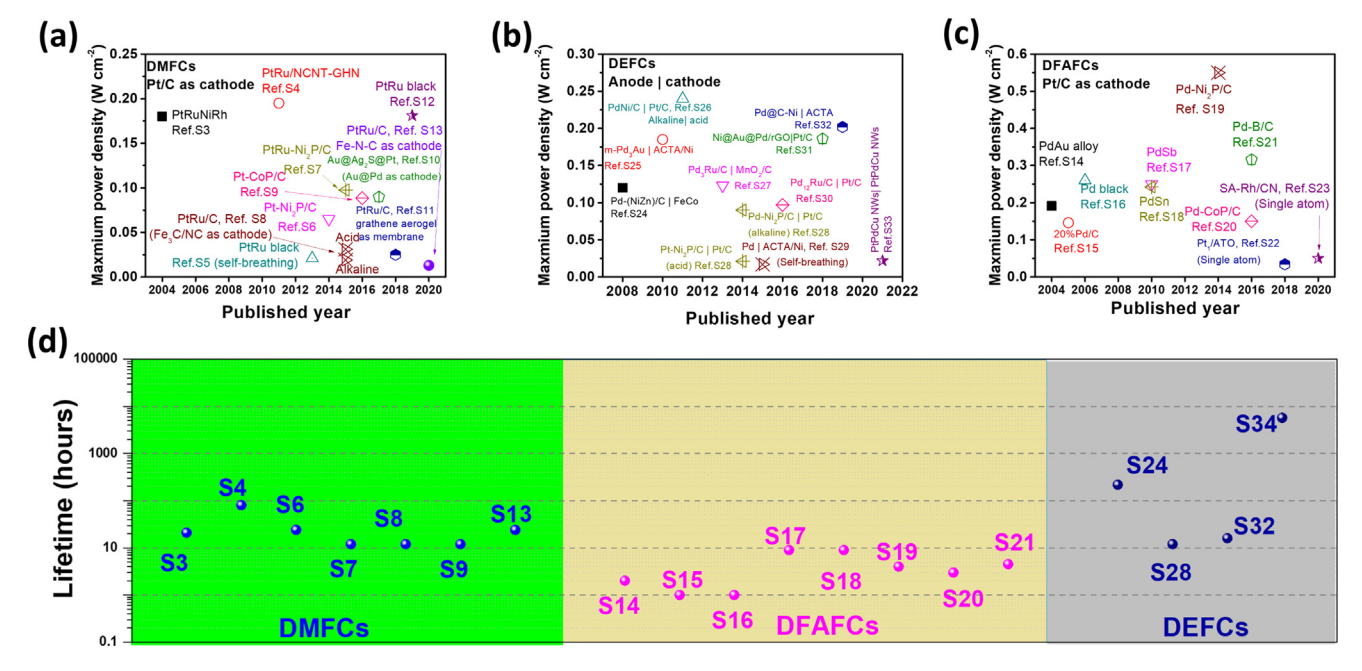


Fig. 6. Current development of catalysts for DLFCs. Maximum power density of (a) direct methanol fuel cells, (b) direct ethanol fuel cells, and (c) direct formic acid fuel cells. The references in (a–c) can be found in Table S2. (d) The lifetime of current fuel cells and the DOE target. The references in (d) can be found in Table S3.

2-e electrocatalysis process. While the cluster and single-atomalloy catalysts are of great interest for MOR and EOR due to the prerequisite of ensemble size. Furthermore, even though only 1-2 atomic sites are needed for the direct pathway for FAOR, most materials in single-atom states (except Pt, Pd, Ir, and Rh SACs) have no electrocatalytic activity for FAOR. Also, different from HOR and other electrochemical reactions employing non-PGMs catalysts, the small organic molecular electrooxidation reactions in DLFCs are highly dependent on PGMs [4]. Thus, the development of non-PGMs-based ADCs materials with cheap metals and alloys is urgently demanded to decrease the cost of the fuel cell system. The current challenges, research directions, and potential strategies for materials preparation, characterizations, and potential application of ADCs for DLFCs are discussed below (Fig. 7).

(I) High throughput and controllable synthesis of ADCs are difficult [61,127,128]. A lot of methods can be used to synthesis ADCs. such as high-temperature pyrolysis, electrochemical deposition, photochemical reduction, wet chemistry method, atomic layer deposition technology, and so on. However, all these methods have their pros and cons [50]. The main questions of ADCs synthesized by the present methods include low productivity, high energy consumption, and inability to scale production. For the anode reactions in the fuel cells, the fine structures needed to catalyze the oxidation of various fuels are quite different. Even though the ADCs show a bright future in various electrochemical applications, they are always designed for specific reactions without one suit for every electrocatalytic system. For alcohol electrooxidation reaction (i.e., MOR and EOR), the requirement of ensemble size should be met to form active sites. While for FAOR, the isolated Pt atoms are sufficient. Moreover, precise control of continuous metal atoms is not easy. To achieve enough active sites, the ADCs loading on the matrix should be as high as it can be [61], which may result in the formation of CCs or NPs instead of ADCs during the synthetic procedure due to the high surface energy.

(II) The ADCs may also tend to aggregate during long-term operation due to the electrochemical Oswald aging [129,130], especially considering that the ADCs have much higher surface energy and chemical potential [131]. Thus, the strong metalsupport effect and anchoring of ADCs on the confined space struc-

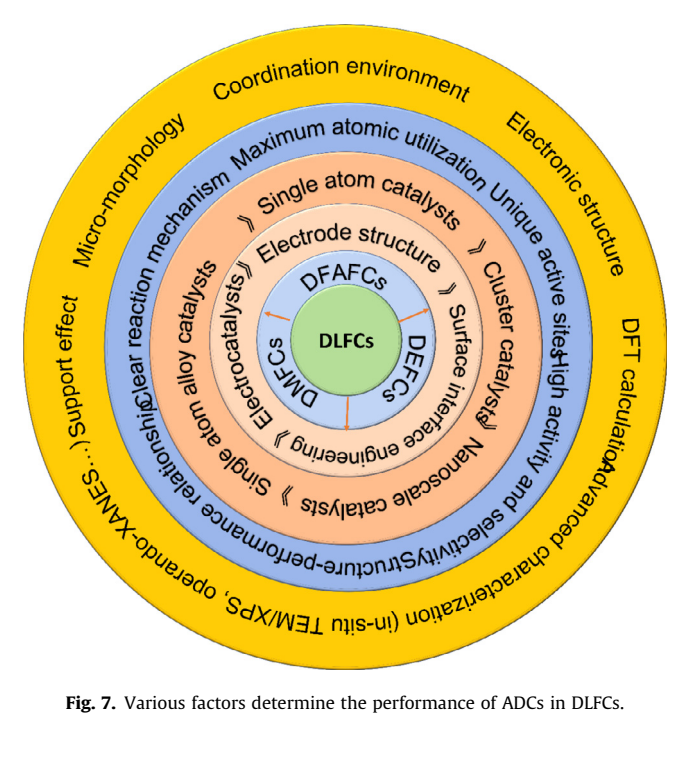


Fig. 7. Various factors determine the performance of ADCs in DLFCs.

tures should be considered. It has been reported that the coordination environment (including coordination number, local structure of the active metal and its electronic interaction with the host. and the electronegativity of the nearest neighbor atoms) of ADCs affects the final performance for many other electrochemical reactions [66,127,132-138]. Little work has been reported on the influence of different coordination environments of ADCs on the anode electrooxidation reactions of DLFCs [56]. Especially for singleatom-alloy and dual-sites coordinated ADCs, the complex coordination environment should be comprehensively understood by combining electrochemical analyses, spectroscopic studies, and theoretical predictions.

(III) The ADCs have a high density of active sites and high surface energy but possibly low stability, especially under a high loading situation, resulting in easy aggregation to form NPs. On the other hand, during long-term operation in the strong acidic/alkaline fuel cells, the ADCs may tend to dissolve and demetallation under such harsh conditions, leading to performance decay [139]. At present, the most widely used supports are carbon-based materials due to the large surface area, good conductivity, plentiful defects, and easily doped by heteroatoms [54-56]. Furthermore, carbon support oxidation/dissolution is still a big challenge for most of the fuel cells [140–143]. Thus, functional supporting materials are recommended [144]. The development of other noncarbon-based functional materials, such as metal or alloy [145], metal oxide [119,146], Mxene [147] TiN [94], ATO [97] with good conductivity is another feasible method [148-152]. However, the main problem of these support materials is the small surface area and high price compared with carbon-based materials. Anchoring the ADCs on these supports is also challenging, which could be addressed by coordinating with heteroatoms to form a strong metal-support interaction. The future research direction will mostly focus on the inexpensive and functional supporting materials (such as carbon-based with high graphitization degree or carbon compounds) with good anti-oxidation/corrosion nature under harsh chemical/electrochemical conditions [153], which should also possess a large surface area, good conductivity, plentiful defects, and easy manipulation to anchor ADCs on the support surface. Besides, the development of catalysts with dual sites/metals should be another efficient way [90], which provides a strong synergistic effect between two sites/metal atoms. Furthermore, developing catalysts with the coexistence of ADCs and NPs should be another new method [91,154], in which the ADCs will address the CO poisoning issues, and NPs promote the small molecule oxidation.

(IV) Advanced real-time characterization techniques should be developed to determine the complex coordination environment. Indeed, the type and coordination environment of the metals have a significant effect on the ADCs' performance [103]. Lowcoordination active sites make it possible for the adsorption of multiple reactants, however, maintaining the stability of the active sites is very difficult due to their high activities. Also, the difficulty in experimentally verifying the precise structures of ADCs largely relies on the DFT to support the proposed reaction activity and pathways. The DFT calculations provide the possible structure of ADCs, which may not be the same as the experimental results directly observed in the actual electrochemical systems. Also, exsitu characterizations cannot capture the real-time information of ADCs during the electrochemical reactions because of the likely surface reconstruction. More in-situ and operando techniques, such as in-situ TEM, in-situ Raman, in-situ FT-IR, in-situ XPS, operando-XAS, and new characterization methods, will be highly recommended to monitor the stability and structure change of ADCs.

(V) Converting the fundamental studies of ADCs to the actual applications in fuel cells is still a big challenge. Most of ADCs show good performance in a half-cell, however, it is difficult to proportionally scale up the performance in the actual fuel cells devices (Fig. 1g, 6a-c). For ADCs, the loading of PMGs on the matrix is very low (typically less than 1 wt%), therefore, enough PGMs are needed to achieve high power and current densities. Thus, the thickness of the catalytic layer in the MEA will be much thicker (at least 5times) than the MEA using the nano-catalysts [155]. The thicker catalytic layer will inhibit the mass transfer and electron transfer, which results in unbalanced and unproportional performance. Even though some pioneering studies have been reported that the ADCs have high electrocatalytic activity for the anode of DLFCs (Table 1), the actual device-level fuel cells are rarely reported. High power densities of ADCs normalized by the weight/mass of PGMs (W mg⁻¹) are usually reported because of the ultra-low loading in the MEA. It would be more reasonable to normalize the power density with the geometric area of MEA (W cm⁻², Fig. 6a-d), which shows the real performance at the level of fuel cells.

(VI) Comprehensively assess the electrocatalytic performance in both half-cell and fuel cells devices. Most ADCs show good performance when tested in a three-electrode half-cell, which is usually much higher than the commercial and benchmarking catalysts. In the three-electrode half-cell systems, the operating conditions, including temperature, humidity, ionic conductivity, and mass transfer, are not the same as the conditions used in the actual fuel cells. Thus, when employed in the actual fuel cells, lower performance is reported (Fig. 1g). In addition to the operating conditions, the way to prepare the electrodes for electrochemical tests is also a reason resulting in different performances [59]. Same to ORR in the cathode of H₂-PEMFCs [126,156], it is recommended to develop a unified standard to assess the catalytic activity, stability, longterm durability, and anti-corrosion property for the anodes of DLFCs. For instance, the binder (such as Nafion or PTFE) content used for preparing MEA should be precisely controlled to optimize the fuel cells' performance. Hence, the macroscopic engineering [157] and technical inquiry of fuel cells using ADCs need to be studied [158]. Additionally, the reasonable design of optimal porosity and nanostructure for catalysts, catalytic layers, and gas diffusion layers are recommended [59]. The micropores are essential for hosting active sites and thus achieving high catalytic activity. While sufficient mesopores and macropores are imperative to ensure effective ionomer distribution for mass transfer of reactants and products. Besides, the fuel crossover is still a big challenge for PEMFCs, thus the development of modified-Nafion membrane or alternative membrane should be a research direction [3]. In parallel, the development of alkaline DLFCs will be another branch, which will reduce the system cost and eliminate the usage of PGMs-dependent catalysts, as well as enhance the material stability and reduce the fuel crossover. However, how to address the low activity of Pt in alkaline solution [159–161] and CO₂ issues [162] should be first considered.

In summary, charming foreground, opportunities, and challenges *co-exist* for the anode electrooxidation in DLFCs using ADCs. By combining high throughput synthetic methods, advanced characterization technologies, theoretical modeling, and fuel cells assembly technology, the intrinsic nature and practical applications of ADCs will be thoroughly understood.

Declaration of Competing Interest

The authors declare that they have no known competing financial interests or personal relationships that could have appeared to influence the work reported in this paper.

Acknowledgments

Y. Yang acknowledges financial supports from the National Science Foundation under Grant Nos. CBET-1949840 and CMMI-

1851674. J.F. Chang acknowledges financial support from the Preeminent Postdoctoral Program (P3) of the University of Central Florida.

Appendix A. Supplementary data

Supplementary data to this article can be found online at https://doi.org/10.1016/j.jechem.2021.12.017.

References

- [1] M.S. Dresselhaus, I.L. Thomas, Nature 414 (2001) 332-337.
- [2] M.K. Debe, Nature 486 (2012) 43-51.
- [3] M.A. Hickner, H. Ghassemi, Y.S. Kim, B.R. Einsla, J.E. McGrath, Chem. Rev. 104 (2004) 4587–4612.
- [4] N. Kakati, J. Maiti, S.H. Lee, S.H. Jee, B. Viswanathan, Y.S. Yoon, Chem. Rev. 114 (2014) 12397–12429.
- [5] C. Bianchini, P.K. Shen, Chem. Rev. 109 (2009) 4183-4206.
- 6] X. Zou, Y. Zhang, Chem. Soc. Rev. 44 (2015) 5148-5180.
- [7] G. Apanel, E. Johnson, Fuel Cells Bull. 2004 (2004) 12-17.
- [8] J.-H. Wee, J. Power Sources 161 (2006) 1–10.
- [9] L. Huang, S. Zaman, X. Tian, Z. Wang, W. Fang, B.Y. Xia, Acc. Chem. Res. 54 (2021) 311–322.
- [10] M. Liu, Z. Zhao, X. Duan, Y. Huang, Adv. Mater. 31 (2019) 1802234.
- [11] Y. Shao, J.P. Dodelet, G. Wu, P. Zelenay, Adv. Mater. 31 (2019) 1807615.
- [12] L. Dai, Y. Xue, L. Qu, H.J. Choi, J.B. Baek, Chem. Rev. 115 (2015) 4823-4892.
- [13] M. Shao, Q. Chang, J.P. Dodelet, R. Chenitz, Chem. Rev. 116 (2016) 3594–3657.
- [14] N. Kimiaie, K. Wedlich, M. Hehemann, R. Lambertz, M. Müller, C. Korte, D. Stolten, Energy Environ. Sci. 7 (2014) 3013–3025.
- [15] J. Chang, L. Feng, C. Liu, W. Xing, X. Hu, Energy Environ. Sci. 7 (2014) 1628– 1632
- [16] J. Chang, L. Feng, C. Liu, W. Xing, X. Hu, Angew. Chem. Int. Ed. 53 (2014) 122–126
- [17] G. Wang, Z. Yang, Y. Du, Y. Yang, Angew. Chem. Int. Ed. 58 (2019) 15848–15854.
- [18] G. Wang, J. Chang, S. Koul, A. Kushima, Y. Yang, J. Am. Chem. Soc. 143 (2021) 11595–11601.
- [19] Z. Li, W. Niu, Z. Yang, N. Zaman, W. Samarakoon, M. Wang, A. Kara, M. Lucero, M.V. Vyas, H. Cao, H. Zhou, G.E. Sterbinsky, Z. Feng, Y. Du, Y. Yang, Energy Environ. Sci. 13 (2020) 884–895.
- [20] M. Luo, Z. Zhao, Y. Zhang, Y. Sun, Y. Xing, F. Lv, Y. Yang, X. Zhang, S. Hwang, Y. Qin, J.Y. Ma, F. Lin, D. Su, G. Lu, S. Guo, Nature 574 (2019) 81–85.
- [21] Z. Liang, L. Song, S. Deng, Y. Zhu, E. Stavitski, R.R. Adzic, J. Chen, J.X. Wang, J. Am. Chem. Soc. 141 (2019) 9629–9636.
- [22] N. Ramaswamy, S. Mukerjee, Chem. Rev. 119 (2019) (1979) 11945–11951.
- [23] J. Chang, L. Feng, K. Jiang, H. Xue, W.-B. Cai, C. Liu, W. Xing, J. Mater. Chem. A 4 (2016) 18607–18613.
- [24] L. Feng, K. Li, J. Chang, C. Liu, W. Xing, Nano Energy 15 (2015) 462–469.
- [25] J. Chang, L. Feng, C. Liu, W. Xing, ChemSusChem 8 (2015) 3340-3347.
- [26] Z. Yao, Z. Wu, M. Hu, S. Alzaim, J. Young, J. Dong, J. Chang, H. Zhuang, E.M. Benchafia, Y. Yang, J. Li, Z. Iqbal, X. Wang, ACS Catal. 11 (2021) 13034–13040.
- [27] J. Chang, T.-J. Ko, M. Je, H.-S. Chung, S.S. Han, M.S. Shawkat, M. Wang, S.J. Park, S.M. Yu, T.-S. Bae, M.-W. Moon, K.H. Oh, H. Choi, Y. Yang, Y. Jung, ACS Energy Lett. 6 (2021) 3481–3487.
- [28] U.S. DOE, https://www.energy.gov/sites/prod/files/2017/05/f34/fcto_myrdd_fuel_cells.pdf (2017).
- [29] A. Wang, J. Li, T. Zhang, Nat. Rev. Chem. 2 (2018) 65–81.
- [30] X. Liu, L. Dai, Nat. Rev. Mater. 1 (2016) 1-12.
- [31] L. An, T.S. Zhao, Y.S. Li, Renew. Sust. Energy Rev. 50 (2015) 1462–1468.
- [32] S.T. Thompson, B.D. James, J.M. Huya-Kouadio, C. Houchins, D.A. DeSantis, R. Ahluwalia, A.R. Wilson, G. Kleen, D. Papageorgopoulos, J. Power Sources 399 (2018) 304–313.
- [33] H.-T. Chung, D.-A. Cullen, D. Higgins, B.-T. Sneed, E.-F. Holby, K.-L. More, P. Zelenay, Science 357 (2017) 479–484.
- [34] M. Li, K. Duanmu, C. Wan, T. Cheng, L. Zhang, S. Dai, W. Chen, Z. Zhao, P. Li, H. Fei, Y. Zhu, R. Yu, J. Luo, K. Zang, Z. Lin, M. Ding, J. Huang, H. Sun, J. Guo, X. Pan, W.A. Goddard, P. Sautet, Y. Huang, X. Duan, Nat. Catal. 2 (2019) 495–503.
- [35] H. Mistry, A.S. Varela, S. Kühl, P. Strasser, B.R. Cuenya, Nat. Rev. Mater. 1 (2016) 1–14.
- [36] Q. Zhang, E. Uchaker, S.L. Candelaria, G. Cao, Chem. Soc. Rev. 42 (2013) 3127–3171.
- [37] I.-E.-L. Stephens, I. Chorkendorf, Science 354 (2016) 1378–1379.
- [38] C. Zhu, S. Fu, Q. Shi, D. Du, Y. Lin, Angew. Chem. Int. Ed. 56 (2017) 13944–13960.
- [39] Y. Lu, W. Chen, Chem. Soc. Rev. 41 (2012) 3594–3623.
- [40] J.A. Fan, C. Wu, K. Bao, J. Bao, R. Bardhan, N.J. Halas, V.N. Manoharan, P. Nordlander, G. Shvets, F. Capasso, Science 328 (2010) 1135–1138.
- [41] J. Zhang, K. Sasaki, E. Sutter, R.R. Adzic, Science 315 (2007) 220–222.
- 42] Y. Chen, S. Ji, C. Chen, Q. Peng, D. Wang, Y. Li, Joule 2 (2018) 1242-1264.
- [43] S. Wei, A. Li, J.C. Liu, Z. Li, W. Chen, Y. Gong, Q. Zhang, W.C. Cheong, Y. Wang, L. Zheng, H. Xiao, C. Chen, D. Wang, Q. Peng, L. Gu, X. Han, J. Li, Y. Li, Nat Nanotechnol 13 (2018) 856–861.
- [44] C.-C. Hou, H.-F. Wang, C. Li, Q. Xu, Energy Environ. Sci. 13 (2020) 1658-1693.

- [45] G. Giannakakis, M. Flytzani-Stephanopoulos, E.C.H. Sykes, Acc. Chem. Res. 52 (2019) 237-247.
- [46] L. Liu, A. Corma, Chem. Rev. 118 (2018) 4981-5079.
- [47] Z. Li, S. Ji, Y. Liu, X. Cao, S. Tian, Y. Chen, Z. Niu, Y. Li, Chem. Rev. 120 (2020) 623-682
- [48] Y. Du, H. Sheng, D. Astruc, M. Zhu, Chem. Rev. 120 (2020) 526-622.
- [49] X. Yang, B. Qiao, J. Li, J. Liu, T. Zhang, Acc. Chem. Res. 46 (2013) 1740-1748.
- [50] L. Zhou, S.Y. Lu, S. Guo, SusMat 1 (2021) 194-210.
- [51] R. Qin, K. Liu, Q. Wu, N. Zheng, Chem. Rev. 120 (21) (2020) 11810–11899.
- [52] Y. Wang, H. Su, Y. He, L. Li, S. Zhu, H. Shen, P. Xie, X. Fu, G. Zhou, C. Feng, D. Zhao, F. Xiao, X. Zhu, Y. Zeng, M. Shao, S. Chen, G. Wu, J. Zeng, C. Wang, Chem. Rev. 120 (2020) 12217-12314.
- [53] B. Qiao, A. Wang, X. Yang, L.F. Allard, Z. Jiang, Y. Cui, J. Liu, J. Li, T. Zhang, Nat. Chem. 3 (2011) 634-641.
- [54] Q. Li, W. Chen, H. Xiao, Y. Gong, Z. Li, L. Zheng, X. Zheng, W. Yan, W.C. Cheong, R. Shen, N. Fu, L. Gu, Z. Zhuang, C. Chen, D. Wang, Q. Peng, J. Li, Y. Li, Adv. Mater. 30 (2018) 1800588.
- [55] H. Shang, X. Zhou, J. Dong, A. Li, X. Zhao, Q. Liu, Y. Lin, J. Pei, Z. Li, Z. Jiang, D. Zhou, L. Zheng, Y. Wang, J. Zhou, Z. Yang, R. Cao, R. Sarangi, T. Sun, X. Yang, X. Zheng, W. Yan, Z. Zhuang, J. Li, W. Chen, D. Wang, J. Zhang, Y. Li, Nat. Commun. 11 (2020) 3049.
- [56] J. Chang, G. Wang, M. Wang, Q. Wang, B. Li, H. Zhou, Y. Zhu, W. Zhang, M. Omer, N. Orlovskaya, Q. Ma, M. Gu, Z. Feng, G. Wang, Y. Yang, Nature Energy 6 (2021) 1144-1153.
- J. Yang, W. Li, D. Wang, Y. Li, Adv. Mater. 32 (2020) 2003300.
- [58] S.K. Kaiser, Z. Chen, D. Faust Akl, S. Mitchell, J. Perez-Ramirez, Chem. Rev. 120 (2020) 11703-11809.
- [59] Y. He, S. Liu, C. Priest, Q. Shi, G. Wu, Chem. Soc. Rev. 49 (2020) 3484-3524.
- [60] T. Zhang, A.G. Walsh, J. Yu, P. Zhang, Chem. Soc. Rev. 50 (2020) 569–588.
- [61] C. Xia, Y. Qiu, Y. Xia, P. Zhu, G. King, X. Zhang, Z. Wu, J.Y. Kim, D.A. Cullen, D. Zheng, P. Li, M. Shakouri, E. Heredia, P. Cui, H.N. Alshareef, Y. Hu, H. Wang, Nat. Chem. 13 (2021) 887-894.
- [62] J. Li, S. Chen, N. Yang, M. Deng, S. Ibraheem, J. Deng, J. Li, L. Li, Z. Wei, Angew. Chem. Int. Ed. 58 (2019) 7035–7039.
- [63] J. Liu, M. Jiao, B. Mei, Y. Tong, Y. Li, M. Ruan, P. Song, G. Sun, L. Jiang, Y. Wang, Z. Jiang, L. Gu, Z. Zhou, W. Xu, Angew. Chem. Int. Ed. 58 (2019) 1163–1167.
- [64] H. Zhang, W. Cheng, D. Luan, X.-W. Lou, Angew. Chem. Int. Ed. 60 (2021) 13177-13196
- [65] Y. Pan, S. Liu, K. Sun, X. Chen, B. Wang, K. Wu, X. Cao, W.C. Cheong, R. Shen, A. Han, Z. Chen, L. Zheng, J. Luo, Y. Lin, Y. Liu, D. Wang, Q. Peng, Q. Zhang, C. Chen, Y. Li, Angew. Chem. Int. Ed. 57 (2018) 8614-8618.
- [66] Y. Gong, L. Jiao, Y. Qian, C. Pan, L. Zheng, X. Cai, B. Liu, S. Yu, H. Jiang, Angew. Chem. Int. Ed. 132 (2020) 2727–2731.
- [67] Y. Wang, F. Chu, J. Zeng, Q. Wang, T. Naren, Y. Li, Y. Cheng, Y. Lei, F. Wu, ACS Nano 15 (2021) 210–239.
- [68] C. Zhu, Q. Shi, S. Feng, D. Du, Y. Lin, ACS Energy Lett. 3 (2018) 1713-1721.
- [69] C. Lu, R. Fang, X. Chen, Adv. Mater. 32 (2020) 1906548.
- [70] J. Zhang, W. Cai, F.X. Hu, H. Yang, B. Liu, Chem. Sci. 12 (2021) 6800–6819.
- [71] R.T. Hannagan, G. Giannakakis, M. Flytzani-Stephanopoulos, E.C.H. Sykes, Chem. Rev. 120 (2020) 12044-12088.
- [72] J.R. Varcoe, R.C.T. Slade, E.L.H. Yee, S.D. Poynton, D.J. Driscoll, J. Power Sources 173 (2007) 194–199.
- [73] H. Bahrami, A. Faghri, J. Power Sources 218 (2012) 286-296.
- [74] O. Muneeb, E. Do, D. Boyd, J. Perez, J.L. Haan, Appl. Energy 235 (2019) 473–479.
- [75] A. Dutta, J. Datta, J. Phys. Chem. C 116 (2012) 25677–25688.
- [76] G. Li, L. Feng, J. Chang, B. Wickman, H. Gronbeck, C. Liu, W. Xing, ChemSusChem 7 (2014) 3374–3381.
- [77] Ş.S.İ. Becerika, F. Kadirgan, J. Electroanal. Chem. 502 (2001) 118–125.
- [78] P.A. Sermon, G.C. Bond, Catal. Rev. 8 (2006) 211-239.
- [79] O.V.K.V.V. Rozanov, Russ. Chem. Rev. 66 (1997) 107-119.
- [80] B.E. Hayden, Acc. Chem. Res. 46 (2013) 1858–1866.
- [81] A. von Weber, S.L. Anderson, Acc. Chem. Res. 49 (2016) 2632–2639. [82] Q. Zhang, J. Guan, Adv. Funct. Mater. 30 (2020) 2000768.
- [83] J. Kim, H.E. Kim, H. Lee, ChemSusChem 11 (2018) 104–113.
- [84] S. Basri, S.K. Kamarudin, W.R.W. Daud, Z. Yaakub, Int. J. Hydrogen Energy 35 (2010) 7957-7970.
- [85] S.M.M. Watanabe, J. Electroanal. Chem. 60 (1975) 275–283.
- [86] A. Hamnettt, Catal. Today 38 (1997) 445–457.[87] B. Gurau, R. Viswanathan, R. Liu, T.J. Lafrenz, K.L. Ley, E.S. Smotkin, E. Reddington, A. Sapienza, B.C. Chan, T.E. Mallouk, S. Sarangapani, J. Phys. Chem. B 102 (1998) 9997–10003.
- M. Yin, Y. Huang, L. Liang, J. Liao, C. Liu, W. Xing, Chem. Commun. 47 (2011) [88] 8172-8174.
- Y. Li, X. Wang, B. Mei, Y. Wang, Z. Luo, E. Luo, X. Yang, Z. Shi, L. Liang, Z. Jin, Z. Wu, Z. Jiang, C. Liu, W. Xing, J. Ge, Sci. Bull. 66 (2021) 1305-1311.
- [90] X. Wang, Y. Li, Y. Wang, H. Zhang, Z. Jin, X. Yang, Z. Shi, L. Liang, Z. Wu, Z. Jiang, W. Zhang, C. Liu, W. Xing, J. Ge, Proc. Natl. Acad. Sci. USA 118 (2021) e2107332118.

- [91] X. Yang, Y. Wang, X. Wang, B. Mei, E. Luo, Y. Li, Q. Meng, Z. Jin, Z. Jiang, C. Liu, J. Ge, W. Xing, Angew. Chem. Int. Ed. 60 (2021) 26177-26183.
- [92] B.D. McNICOL, J. Electroanal. Chem. 118 (1981) 71-87.
- [93] Y.T. Kim, K. Ohshima, K. Higashimine, T. Uruga, M. Takata, H. Suematsu, T. Mitani, Angew. Chem. Int. Ed. 45 (2006) 407-411.
- [94] S. Yang, J. Kim, Y.J. Tak, A. Soon, H. Lee, Angew. Chem. Int. Ed. 55 (2016) 2058-2062
- [95] S. Sun, G. Zhang, N. Gauquelin, N. Chen, J. Zhou, S. Yang, W. Chen, X. Meng, D. Geng, M.N. Banis, R. Li, S. Ye, S. Knights, G.A. Botton, T.-K. Sham, X. Sun, Sci. Rep. 3 (2013) 1-9.
- [96] J. Liu, F.R. Lucci, M. Yang, S. Lee, M.D. Marcinkowski, A.J. Therrien, C.T. Williams, E.C. Sykes, M. Flytzani-Stephanopoulos, J. Am. Chem. Soc. 138 (2016) 6396-6399.
- [97] J. Kim, C.-W. Roh, S.K. Sahoo, S. Yang, J. Bae, J.W. Han, H. Lee, Adv. Energy Mater. 8 (2018) 1701476.
- [98] S. Yang, H. Lee, ACS Catal. 3 (2013) 437-443.
- [99] A.E. Russell, Faraday Discussions 140 (2008) 363-378.
- [100] R. Subbaraman, D. Tripkovic, D. Strmcnik, K.-C. Chang, M. Uchimura, V. Stamenkovic, N.-M. Markovic, Science 334 (2011) 1256-1260.
- [101] N.-D. Tran, M.-F. Camellone, S. Fabris, J. Phys. Chem. C122 (2018) 17917-17927.
- [102] M.-D. Marcinkowski, S.-F. Yuk, N. Doudin, R.-S. Smith, M.-T. Nguyen, B.-D. Kay, V.-A. Glezakou, R. Rousseau, Z. Dohnálek, ACS Catal. 9 (2019) 10977–10982.
- [103] S. Mitchell, J. Perez-Ramirez, Nat. Commun. 11 (2020) 4302.
- [104] E. Antolini, J. Power Sources 170 (2007) 1-12.
- [105] C. Yang, P. Costamagna, S. Srinivasan, J. Benzigerc, A.B. Bocarsly, J. Power Sources 103 (2001) 1-9.
- [106] I. Kim, O.H. Han, S.A. Chae, Y. Paik, S.H. Kwon, K.S. Lee, Y.E. Sung, H. Kim, Angew. Chem. Int. Ed. 50 (2011) 2270-2274.
- [107] R. Kavanagh, X.M. Cao, W.F. Lin, C. Hardacre, P. Hu, Angew. Chem. Int. Ed. 51 (2012) 1572-1575.
- [108] N. Fujiwara, Z. Siroma, S.-I. Yamazaki, T. Ioroi, H. Senoh, K. Yasuda, J. Power Sources 185 (2008) 621-626.
- [109] W.J. Zhou, B. Zhou, W.Z. Li, Z.H. Zhou, S.Q. Song, G.Q. Sun, Q. Xin, S. Douvartzides, M. Goula, P. Tsiakaras, J. Power Sources 126 (2004) 16-22.
- [110] S. Song, W. Zhou, Z. Zhou, L. Jiang, G. Sun, Q. Xin, V. Leontidis, S. Kontou, P. Tsiakaras, Int. J. Hydrogen Energy 30 (2005) 995-1001.
- [111] A. von Weber, E.T. Baxter, S. Proch, M.D. Kane, M. Rosenfelder, H.S. White, S.L. Anderson, Phys. Chem. Chem. Phys. 17 (2015) 17601-17610.
- [112] R. Ding, X. Wu, G. Han, Q. Wang, H. Lu, H. Li, A. Fu, P. Guo, ChemElectroChem 2 (2015) 427-433.
- [113] R. Liu, L.Q. Zhang, C. Yu, M.T. Sun, J.F. Liu, G.B. Jiang, Adv. Mater. 29 (2017) 1604571.
- [114] A. Kowal, M. Li, M. Shao, K. Sasaki, M.B. Vukmirovic, J. Zhang, N.S. Marinkovic, P. Liu, A.I. Frenkel, R.R. Adzic, Nat. Mater. 8 (2009) 325–330.
- [115] S. Luo, L. Zhang, Y. Liao, L. Li, Q. Yang, X. Wu, X. Wu, D. He, C. He, W. Chen, Q. Wu, M. Li, E.J.M. Hensen, Z. Quan, Adv. Mater. 33 (2021) 2008508.
- [116] C. Xu, P.K. Shen, Y. Liu, J. Power Sources 164 (2007) 527-531.
- [117] E. Antolini, E.R. Gonzalez, J. Power Sources 195 (2010) 3431-3450.
- [118] Z. Yang, Y. Wang, M. Zhu, Z. Li, W. Chen, W. Wei, T. Yuan, Y. Qu, Q. Xu, C. Zhao, X. Wang, P. Li, Y. Li, Y. Wu, Y. Li, ACS Catal. 9 (2019) 2158–2163.
- [119] Y. Zhu, J. Zhang, J. Jin, J. Sun, H. Tang, Q. Chen, Z. Zhang, W. Sun, G. Meng, Q. Xu, Y. Zhu, A. Han, L. Gu, D. Wang, Y. Li, Nat. Commun. 12 (2021) 5273.
- [120] R.S. Jayashree, J.S. Spendelow, J. Yeom, C. Rastogi, M.A. Shannon, P.J.A. Kenis, Electrochim. Acta 50 (2005) 4674-4682.
- [121] M. Neurock, M. Janik, A.A. Wieckowski, Faraday Discuss. 140 (2008) 363–378.
- [121] M. Nediock, M. Jalin, M. Wickerski, Landan, J. School, J. Yuan, T. Regier, A. Aldalbahi, Z. Almarhoon, S. Chen, D.E. Jiang, N. Zheng, P. Zhang, Nat. Mater. 17 (2018) 1033-1039.
- [123] Y. Lu, C. Zhang, X. Li, A.R. Frojd, W. Xing, A.Z. Clayborne, W. Chen, Nano Energy 50 (2018) 316-322.
- [124] Z. Li, Y. Chen, S. Ji, Y. Tang, W. Chen, A. Li, J. Zhao, Y. Xiong, Y. Wu, Y. Gong, T. Yao, W. Liu, L. Zheng, J. Dong, Y. Wang, Z. Zhuang, W. Xing, C.T. He, C. Peng, W. C. Cheong, Q. Li, M. Zhang, Z. Chen, N. Fu, X. Gao, W. Zhu, J. Wan, J. Zhang, L. Gu, S. Wei, P. Hu, J. Luo, J. Li, C. Chen, Q. Peng, X. Duan, Y. Huang, X.M. Chen, D. Wang, Y. Li, Nat. Chem. 12 (2020) 764-772.
- [125] Y. Xiong, J. Dong, Z.Q. Huang, P. Xin, W. Chen, Y. Wang, Z. Li, Z. Jin, W. Xing, Z. Zhuang, J. Ye, X. Wei, R. Cao, L. Gu, S. Sun, L. Zhuang, X. Chen, H. Yang, C. Chen, Q. Peng, C.R. Chang, D. Wang, Y. Li, Nat. Nanotechnol. 15 (2020) 390–397.
- [126] U.S. DOE, https://www.energy.gov/eere/fuelcells/doe-technical-targetspolymer-electrolyte-membrane-fuel-cell-components, (2020).
- [127] H. Xu, D. Cheng, D. Cao, X.C. Zeng, Nat. Catal. 1 (2018) 339–348.
 [128] H. Fei, J. Dong, Y. Feng, C.S. Allen, C. Wan, B. Volosskiy, M. Li, Z. Zhao, Y. Wang, H. Sun, P. An, W. Chen, Z. Guo, C. Lee, D. Chen, I. Shakir, M. Liu, T. Hu, Y. Li, A.I. Kirkland, X. Duan, Y. Huang, Nat. Catal. 1 (2018) 63-72.
- [129] T.W. Hansen, A.T. DeLaRiva, S.R. Challa, A.K. Datye, Acc. Chem. Res. 46 (2013) 1720-1730.
- [130] A. Kregar, A. Kravos, T. Katrašnik, Fuel Cells 20 (2020) 487-498.
- [131] F.N. Büchi, M. Inaba, T.J. Schmidt (Eds.), Polymer Electrolyte Fuel Cell Durability, Springer New York, New York, NY, 2009.

- [132] W. Yang, M. Zhao, X. Ding, K. Ma, C. Wu, I.D. Gates, Z. Gao, Phys. Chem. Chem. Phys. 22 (2020) 3983–3989.
- [133] T. Sun, S. Mitchell, J. Li, P. Lyu, X. Wu, J. Perez-Ramirez, J. Lu, Adv. Mater. 33 (2020) 2003075.
- [134] X. Li, H. Rong, J. Zhang, D. Wang, Y. Li, Nano Res. 13 (2020) 1842–1855.
- [135] J. Zhang, Y. Zhao, C. Chen, Y.C. Huang, C.L. Dong, C.J. Chen, R.S. Liu, C. Wang, K. Yan, Y. Li, G. Wang, J. Am. Chem. Soc. 141 (2019) 20118–20126.
- [136] Z. Jakub, J. Hulva, M. Meier, R. Bliem, F. Kraushofer, M. Setvin, M. Schmid, U. Diebold, C. Franchini, G.S. Parkinson, Angew. Chem. Int. Ed. 58 (2019) 13961–13968.
- [137] X.P. Yin, H.J. Wang, S.F. Tang, X.L. Lu, M. Shu, R. Si, T.B. Lu, Angew. Chem. Int. Ed. 57 (2018) 9382–9386.
- [138] Y. Xu, M. Chu, F. Liu, X. Wang, Y. Liu, M. Cao, J. Gong, J. Luo, H. Lin, Y. Li, Q. Zhang, Nano Lett. 20 (2020) 6865–6872.
- [139] L.M. Roen, C.H. Paik, T.D. Jarvi, Electrochem. Solid. St. Lett. 7 (2004) A19.
- [140] S. Maass, F. Finsterwalder, G. Frank, R. Hartmann, C. Merten, J. Power Sources 176 (2008) 444–451.
- [141] Y. Hu, P. Wu, Y. Yin, H. Zhang, C. Cai, Appl. Catal. B: Environ. 111–112 (2012) 208–217.
- [142] B. Avasarala, R. Moore, P. Haldar, Electrochim. Acta 55 (2010) 4765-4771.
- [143] J. Chang, G. Wang, Y. Yang, Small Sci. 1 (2021) 2100044.
- [144] Y.J. Wang, D.P. Wilkinson, J. Zhang, Chem. Rev. 111 (2011) 7625-7651.
- [145] F. Pan, Z. Li, Z. Yang, Q. Ma, M. Wang, H. Wang, M. Olszta, G. Wang, Z. Feng, Y. Du, Y. Yang, Adv. Energy Mater. 11 (2020) 2002204.
- [146] Q. Wang, X. Huang, Z.L. Zhao, M. Wang, B. Xiang, J. Li, Z. Feng, H. Xu, M. Gu, J. Am. Chem. Soc. 142 (2020) 7425–7433.
- [147] J. Zhang, Y. Zhao, X. Guo, C. Chen, C.-L. Dong, R.-S. Liu, C.-P. Han, Y. Li, Y. Gogotsi, G. Wang, Nat. Catal. 1 (2018) 985–992.
- [148] M. Zhu, C. Zhao, X. Liu, X. Wang, F. Zhou, J. Wang, Y. Hu, Y. Zhao, T. Yao, L.-M. Yang, Y. Wu, ACS Catal. 11 (2021) 3923–3929.
- [149] M. Zhu, J. Wang, W. Wu, Chem. Res. Chinese U. 36 (2020) 320-328.
- [150] W. Guo, Z. Wang, X. Wang, Y. Wu, Adv. Mater. 33 (2021) 2004287.
- [151] Y. Wang, D. Wang, Y. Li, J. Energy Chem. 65 (2022) 103–115.
- [152] J. Yang, W. Li, D. Wang, Y. Li, Small Structures 2 (2020) 2000051.
- [153] H.F. Wang, L. Chen, H. Pang, S. Kaskel, Q. Xu, Chem. Soc. Rev. 49 (2020) 1414– 1448
- [154] L. Chong, J. Wen, J. Kubal, F.G. Sen, J. Zou, J. Greeley, M. Chan, H. Barkholtz, W. Ding, D.-J. Liu, Science 362 (2018) 1276–1281.
- [155] K. Kodama, T. Nagai, A. Kuwaki, R. Jinnouchi, Y. Morimoto, Nat. Nanotechnol. 16 (2021) 140–147.
- [156] J.S. Spendelow https://www.hydrogen.energy.gov/pdfs/review18/fc161_ spendelow_2018_o.pdf.
- [157] G. Deng, L. Liang, C. Li, J. Ge, C. Liu, Z. Jin, W. Xing, J. Power Sources 427 (2019) 120–128.
- [158] G. Deng, L. Liang, Z. Jin, C. Li, C. Liu, J. Ge, W. Xing, AIChE J. 64 (2018) 3519–3528.
- [159] J. Durst, A. Siebel, C. Simon, F. Hasché, J. Herranz, H.A. Gasteiger, Energy Environ. Sci. 7 (2014) 2255–2260.
- [160] W. Sheng, H.A. Gasteiger, Y. Shao-Horn, J. Electrochem. Soci. 157 (2010) B1529.
- [161] J. Zheng, W. Sheng, Z. Zhuang, B. Xu, Y. Yan, Sci. Adv. 2 (2016) e1501602.
- [162] B. Cermenek, J. Ranninger, V. Hacker, Ethanol: Science and Engineering, Elsevier, Amsterdam, 2019, pp. 383–405.



Jinfa Chang completed his Ph.D. degree in physical chemistry from the Chinese Academy of Sciences, Changchun Institute of Applied Chemistry in 2018. He joined Prof. Yang's group as a postdoctoral researcher supported by the Preeminent Postdoctoral Program (P3) in April 2019. His research interests focus on electrochemical energy storage and conversion, especially in the fields of fuel cells, metal-air batteries, and water splitting.



Guanzhi Wang completed her Bachelor's degree in material science at Shandong University in 2016. She is currently a doctoral student in Prof. Yang's group at NanoScience Technology Center, University of Central Florida. Her research mainly focuses on the design and fabrication of nanoporous alloy films for electrochemical energy storage and conversion technologies.



Wei Zhang completed his Bachelor's degree in materials physics at Hunan University in 2016 and obtained his Master's degree in materials science & engineering at University of Florida in 2018. He is currently a Ph.D. student in Prof. Yang's group at NanoScience Technology Center, University of Central Florida. His research interests include thin-film fabrication for electrochemical devices and energy conversion and storage technology.



Yang Yang is an associate professor at the University of Central Florida. His research focuses include surface and interface electrochemistry of energy materials and devices, materials science, nanomanufacturing, electrochemical engineering, and nanoscience technology. His homepage website is http://www.yangyanglab.com.